33

Osteoporosis: A Look at the Future

Iliyan Kolev[1], Lyudmila Ivanova[1], Leni Markova[1],
Anelia Dimitrova[2], Cyril Popov[3] and Margarita D. Apostolova[1]
[1]*Medical and Biological Research Lab, Institute of Molecular Biology, Bulgarian Academy of Sciences, Sofia,*
[2]*Department of Physiology and Pathophysiology, Medical University, Pleven,*
[3]*Institute of Nanostructure Technologies and Analytics, University of Kassel,*
[1,2]*Bulgaria*
[3]*Germany*

1. Introduction

Osteoporosis – the commonest age-related skeletal chronic disorder– is characterized by loss of bone mass, alterations of bone micro-architecture, and increased fracture risk. It has, however, received much less attention than most chronic diseases. Osteoporotic fractures are expensive to treat, and cause significant mortality, morbidity, and loss of independence in an ever broader population of patients. As we have said, osteoporosis is a disease in which the mineral density of the bone (BMD) is reduced, its microarchitecture disrupted, and the expression profile of non-collagenous proteins altered. All these factors predispose bones to fractures, particularly the hip, spine and wrist, and are a major cause of disability, severe back pain and deformity. The World Health Organization estimates that approximately 70 million people worldwide have osteoporosis (Penrod J. et al., 2008). The total cost of osteoporosis is difficult to calculate because it includes in-patient and out-patient medical care, loss of working days, chronic nursing-home costs, and medication. The direct costs of osteoporosis arise mainly from the management of patients with hip fractures. Hip fractures also account for 40% of all deaths from trauma in patients over 75, with 68% of all patients not returning to their former level of activity following an osteoporotic hip fractures. The annual worldwide incidence of hip fracture is 1.5 million, a number projected to grow to 2.6 million by 2025 and to 4.5 million by 2050 (Penrod J. et al., 2008). For these reasons, it is necessary to pay a special attention to these health problems which disturb the quality of life.

1.1 Evidence for genetic variation influencing fractures

Both disease prevention and innovation in therapy are critically dependent on identifying the factors that predispose to the development of osteoporosis (Marini & Brandi, 2010). Several studies that have investigated the influence of genetic factors on the development of osteoporosis have found a weaker contribution than to peak bone mass where up to 80% of

the variance can be explained by genetics alone in both sexes (Ralston & de Crombrugghe, 2006).

High-throughput technologies facilitate the identification of genetic, genomic, proteomic, and metabolomic markers of osteoporosis risk that may find a place in clinical prediction algorithms. The operation of intricate networks of genes, environmental factors, and gene-by-environmental interactions further complicate our understanding of the genetic components of the osteoporosis. Until recently, single nucleotide polymorphisms (SNPs) were thought to be the predominant form of genomic variation and to account for phenotypic variation in patients with osteoporotic disorders and those without. However, with the advent and application of array-based comparative genomic hybridization (aCGH), which allows analysis of the genome with a significantly higher resolution than previously possible, scientists have demonstrated that humans are much more genetically variable than previously thought. In two different publications in 2004 (Iafrate et al., 2004; Sebat et al., 2004) hundreds of genomic regions that varied significantly with respect to the number of copies (CNVs) have been reported. Since then, older observations (Iafrate et al., 2004; Sebat et al., 2004) have been replicated and expanded (Conrad et al., 2006; deVries et al., 2005; Repping et al., 2006; Schoumans et al., 2005; Sharp et al., 2005; Tuzun et al., 2005). CNVs vary greatly in size, with insertions or deletions ranging from below 1 kb to several Mb in length (Feuk et al., 2006). As with other types of genetic variation, some gene CNVs have been associated with susceptibility or resistance to disease (Aitman et al., 2006; Cappuzzo et al., 2005; Feuk et al., 2006; Gonzalez et al., 2005; Redon et al., 2006; Sebat et al., 2007; Deng et al., 2010). In humans, CNVs encompass more DNA than SNPs and may be responsible for a substantial part of human phenotypic variability and disease susceptibility (Freeman et al., 2006; Redon et al., 2006). In spite of revolutionary technologies, the major genes determining the bone density and the fracture risk in humans remain uncertain. Approximately 150 candidate genes that might influence the BMD have been identified (Richards et al., 2009; Zhang et al., 2010). Confirmation analyses have revealed that only 30 of these SNPs are somehow connected with the development of osteoporosis.

Preliminary Pathway analysis (Molecular INTeraction database) of the differentially regulated genes/proteins in patients with osteoporosis (Richards et al., 2009) has revealed significance for the highlighted nodes (Mothers against decapentaplegic homolog (SMAD) 2, 3, 4 and 7, Tumor necrosis factor superfamily (TNFRSF), Integrin beta-3 (ITGB3), Bone morphogenetic proteins (BMPs), Transforming growth factor beta-receptors (TGFBRs), Calmodulin 3 (CALM3), TANK protein, Cystic fibrosis transmembrane conductance regulator (CFTR), Pro-neuropeptide Y (NPY)), suggesting that these pathways might play a concomitant role in the pathogenesis of osteoporosis (Fig. 1). New findings notwithstanding, we have to remember that the formation of bone and its repair is a complex process including skeletal patterning, remodeling, and bone growth. The rate of bone formation is dependent on the commitment and replication of several cell types, including osteoprogenitor cells. Their differentiation into functional osteoblasts and the life span of mature osteoblasts is very important. Although a few signaling pathways and patterns of gene expression have been identified in the process of osteoblast differentiation, the exact molecular mechanisms are poorly understood.

A recent genome wide association study (GWAS) has identified approximately 9000 CNVs in patients with lower BMD at spine, hip, and femoral neck (Deng et al., 2010). This study showed that only one low copy number variant of VPS13B gene had some possible

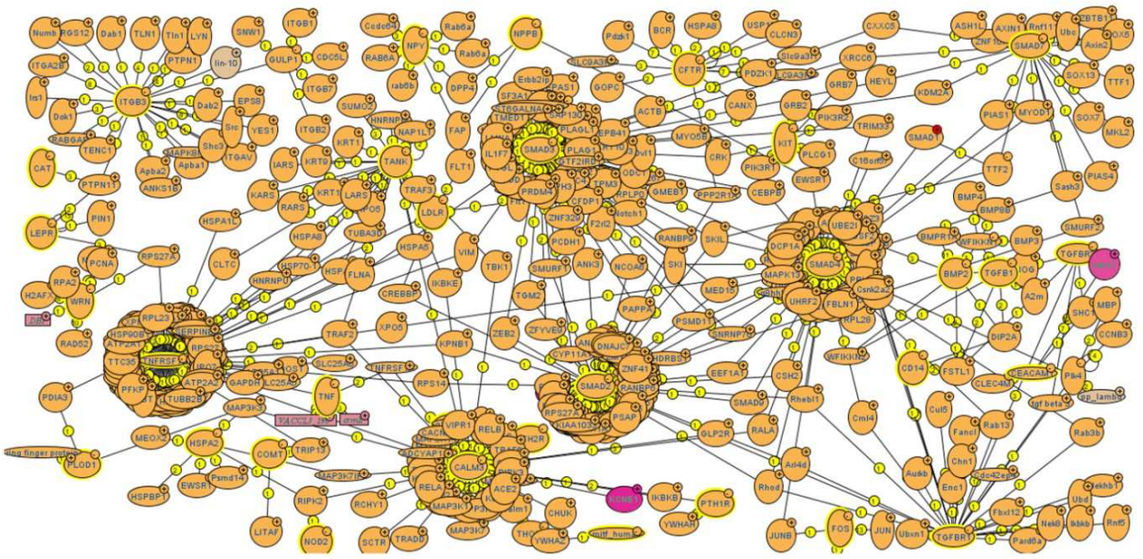

Fig. 1. Overview of signal-transduction pathways associated with candidate genes underlying susceptibility to osteoporosis.

protective role associated with stronger bones and reducing the risk of osteoporotic fractures. The extent to which genes cause alteration in combination with different risk factors for fracture might explain the incidence of fractures in the population, and will depend on strength of association between the risk factor and fracture risk, and on proportion of the population at different levels of allele frequencies (Hopper, 2000). Therefore, although a variation in a risk factor may be strongly genetically determined, it may have little consequence for the disease in terms of explaining different patient's clinical outcomes.

2. State-of-the-art

Bone fracture healing is a complicated, multistage process, influenced by cells events and regulated by local and systematic factors. Recent data concerning the regulatory factors correlated with fracture healing suggest that several chemical compounds can be used to stimulate bone growth, and enhance callus formation and maturation. The pharmacological approach towards osteoporosis prevention aims to increase the bone mass by decreasing of osteoclastic bone resorption with the aid of estrogens, bisphosphonates, calcitonin, calcium plus, cholecalciferol, calcitriol and selective estrogen receptor modulators (Grabo & Longyhore, 2008).

Moving away from these conventional approaches, investigators have recently used lovastatin loaded nanoparticles (Garrett et al., 2007) or Ossein – Hydroxyapatit compounds (OHC) for osteoporosis treatment. One of the most important pleiotropic actions of statins is their effect on bone metabolism (Horiuchi & Maeda, 2006). Statins form a class of hypolipidemic agents, known as 3-hydroxy-3-methylglutaryl coenzyme A (HMG Co-A) reductase inhibitors, commonly used as therapy to lower the cholesterol levels in people with/or at risk of cardiovascular disease. Statins exhibit a pleiotropic effect in preclinical models, accelerating fracture healing and increasing angiogenesis when the fracture area is

systemically or locally treated. OHCs also have osteogenic and chondrogenic properties *in vitro* and accelerate fracture healing *in vivo* (Annefeld et al., 1986).

Some patients respond poorly to these therapies, including the integration of implants such as hip replacements. They develop post-surgical complications, caused mainly by weakening of the implant-bone bond due to bone resorption at the interface. This is caused by necrosis of the surrounding host tissue due to surgery, heat released during cement polymerization and micromotion caused by poor fixation. To improve the integration of implants with weak osteoporotic bone, fixation augmentation techniques have been recently proposed such as superficial coatings of polymethylmethacrylate, calcium phosphate ceramics or hydroxyapatite (HA) onto the metallic surfaces (Annefeld et al., 1986; Moroni et al., 2001; Moroni et al., 2005a; Moroni et al., 2005b). Metal surfaces coated with nanohydroxyapatite or biomimetic calcium phosphate (CaP) have been used to improve the fracture fixation stability, which has been proposed as a strategy for porous bones. However, the conventional method for CaP-coating requires high temperature treatment, which prevents the addition of bioactive pharmaceuticals. Post-treatment loading with drugs generally results in their uncontrolled, high kinetic release. A biomimetic nano-CaP coating technology which retains all the features of plasma spraying, including controllable porosity and 3D morphology was recently developed. This technology results in the deposition of amorphous CaP coprecipitated with bioactive substances through the full thickness of the coating, allowing gradual release. The influence of resorbable CaP particles and paste on bone healing was investigated by Bloemers et al. (Bloemers et al., 2003). Twelve weeks after the defect reconstruction, radiological, biomechanical, and histological analyses were performed. Biomechanical tests showed a significantly higher torsional stiffness for the resorbable CaP paste group when compared with the autologous bone.

Several other investigations (de Melo et al., 2006; Niemeyer et al., 2010) published recently utilized the transplantation of xenogenic human and autologous ovine mesenchymal progenitor cells in an ovine critical-size defect or study whether blood-derived endothelial progenitor cells promote the bone regeneration once transplanted into an ovine and tibial defect in animal models (Rozen et al., 2009). Both studies showed significant bone regenerative processes, but the overall results are inconclusive.

Nanoscale materials currently investigated for bone tissue engineering applications can be placed in the following categories: ceramics, metals, and composites. Each type has distinct properties that can be advantageous for specific bone repairing applications. For example, HA, an inorganic compound of bone can be made synthetically. Ceramics are not mechanically tough enough to be used in bulk for large scale bone fractures. However, for a long time they have found applications as bioactive coatings, owing to their ionic bonding mechanisms that are favorable for osteoblast functions (Hench, 1982; Hench, 2004). Unlike ceramic materials, metals are not present in the body as bulk materials. However, because of their mechanical strength and relative inactivity with biological substances, metals and alloys (Ti, Ti_6Al_4V, CoCrMo, etc.) have been the materials of choice for large bone fractures. Composites of the above mentioned materials can be synthesized to provide a wide range of material properties and also to increase the bone implant performance (Nikolovski & Mooney, 2000). It was found that detonation-generated nanodiamond (DND) inclusions can stimulate the biological performance of the composite layer (Pramatarova et al., 2007).

Although novel bioactive and organic materials with good bioavailability and osteogenic activity such as new nano CaP and sulfate cements, bioactive glass and polymers, have been

developed in last years, their application in the treatment of osteoporotic bones is limited because of their weak angiogenic properties.

3. New concepts and strategies for the treatment of osteoporosis

A significant number of osteoporotic bone fractures are treated with implants which are generally fixed with bone cement. However, this fixation requires good quality cancellous bone, generally absent in the osteoporotic population. The incidence of implant loosening and revision surgery is high when osteoporosis is present. For years, attempts have been made to use tissue engineering to develop functional substitutes for damaged or diseased tissues through complex constructs with living cells, bioactive molecules and three-dimensional scaffolds, which can support cell attachment, proliferation and differentiation. By integrating of nanotechnology with cellular and molecular biology we aimed to develop injectable, bioresorbable polymers, in acellular and autologous cell-seeded forms, to enhance the bone fracture fixation and healing, and to promote regeneration of the natural tissue.
New strategies involve:

- Preparation of injectable scaffolds
  - Incorporation of angiogenic/osteogenic factors within the scaffolds (if necessary)
  - Homogeneous distribution within a cavity of any shape
  - Easy integration of biologically active substances and nanomaterials for improvement of the pro-angiogenetic properties of bone macroporous scaffolds
  - The ability to deliver progenitor cells as autologous transplant
  - Manipulation of cell function
  - Avoidance of foreign body reactions
  - Transplant assimilation and remodelling
- Preparation of implants with tailored properties
  - Enhancing minimally invasive application and securing better apposition between bone tissue and material
  - Deposition of angiogenic extracellular matrixes on the surfaces
  - Preparation of new implants with increased biocompatibility by specific nanocoating technology.

Strategies that allow efficient scaffold injectability are critical for the realization of successful treatment for osteoporosis with minimally invasive surgery.

4. Methods

4.1 Synthesis of PLGA-PEG-PLGA triblock copolymers

The synthesis of block copolymers with a general structure PLGA-PEG-PLGA was accomplished as follows: A mixture of polyethylene glycol (PEG), lactide and glycolide with a predetermined molar ratio (Table 1) was placed into a polymerization flask and dried by azeotropic distillation using anhydrous toluene as an entraining agent. After heating at 80 °C under stirring, 0.5 mL of 0.06 M $Sn(Oct)_2$ was rapidly injected through a septum into the polymerization mixture. Then the reaction temperature was elevated to 140 °C and maintained constant for 24 hours. After that, the polymerization flask was cooled down to room temperature and the reaction mixture was dissolved in a small amount of CH_2Cl_2. The copolymers were collected by precipitation in cooled diethyl ether and dried at 40 °C in vacuum for few minutes. The obtained copolymers were dissolved in cold water and then

heated to 80 °C to precipitate, and remove the water-soluble impurities and unreacted polyethylene oxide. The purification process was repeated three times.

Sample	Lactide, g	Glycolide, g	PEG, g	Yield,%
$PLGA_{1000}$-PEG_{1000}-$PLGA_{1000}$	8.352	1.665	5.000	97
$PLGA_{900}$-PEG_{1000}-$PLGA_{900}$	7.500	1.499	5.000	93
$PLGA_{800}$-PEG_{1000}-$PLGA_{800}$	6.665	1.330	5.000	98
$PLGA_{700}$-PEG_{1000}-$PLGA_{700}$	5.832	1.165	5.000	87

Table 1. The starting monomer and oligomer amounts for the synthesized block copolymers and their yields.

The polymers were characterized by ^1H NMR (250 MHz) spectroscopy recorded with a Bruker Avance DRX 250 apparatus, Fourier transforms infrared (FTIR) spectroscopy, and Size exclusion chromatography (GPC). GPC was performed on Waters chromatographic system, equipped with a double detection- differential refractometer M410 and M484 UV detector. Data collection and processing were done using Clarity software. The analyses were performed on Ultrastyragel Linear**,** Styragel 100 Å**,** and Styragel 500 Å columns (Waters) calibrated with polyethylene oxide (PEO) standards. Tetrahydrofuran was used as mobile phase with a flow rate of 1.0 ml/min at 45 °C. FTIR spectra (KBr pallets) were recorded on Bruker-Vector 22 FTIR spectrometer at a resolution of 1-2 cm^{-1} accumulating 50 scans.

4.2 Nanocrystalline diamonds production and characterization

Shock-wave synthesis was used to produce nanocrystalline diamonds **(**NCDs) by explosive conversion of a trinitrotoluene/hexogene mixture with negative oxygen balance (Ivanova et al., 2011). A water-cooled combustion chamber with 3.0 m^3 volume was applied. A mixture of diamond blends containing 85% NCDs was obtained. The NCDs were purified by oxidative removal of the non-diamond carbon using a mixture of $K_2Cr_2O_7$ and H_2SO_4 according to (Tsoncheva et al., 2006). NCDs were characterized by X-ray diffraction (XRD), transmission electron microscopy (TEM), and energy dispersive X-ray spectroscopy (EDS). The XRD spectra were obtained with a Bruker D2Phaser diffractometer with CuKα radiation in 2 theta range between 30 and 110° with a step of 0.02° and a measuring time of 10 s per point. The size and morphology of NCDs were studied by TEM. The experiments were performed with a Philips EM420 transmission electron microscope with accelerating voltage of 120 kV. The sample was suspended by ultrasonic agitation in ethanol at room temperature and an aliquot of the solution was dropped on a holey carbon film supported on a copper grid. The impurities present in the samples were analyzed with an EDAX 9100/70 attached to the microscope.

4.3 Preparation of polymer hydrogels and its lovastatin and NCD loaded forms

The polymer hydrogels were obtained by dissolving of the PLGA-PEG-PLGA polymers in deionized water at suitable temperatures - below and above the so-called "gelation temperature". Equal amounts of freeze-dried PLGA-PEG-PLGA polymers were dissolved in different amounts of sterile water to prepare samples with desired concentrations (10, 15, 20, and 25% (w/w)). The total solubility of the copolymers was achieved by continuous shaking of

the samples at a temperature of 4.0 °C for 48 h. The gel-sol transition behavior of the block copolymer solutions was investigated following the procedure described by Lee et al. (Lee et al., 2006) using a WB-4MS water bath-thermostat (Biosan) and also was studied by rheological analysis (Yu et al., 2010). The introduction of NCDs in the polymer hydrogels was made by preparation of sterile aqueous NCD suspensions with different concentrations, used in order to get a final concentration of 0.5 mg/ml in the hydrogels. The sterilization of the NCDs was achieved through stepwise washing with 99% and 45% ethanol and autoclaved deionized water. Lovastatin loaded hydrogels were obtained by dissolution of lovastatin (powder) in the already prepared hydrogels. The final concentration of lovastatin was 825 μM.

4.4 *In vitro* degradation of the polymeric hydrogels

The degradation of the polymeric hydrogels (166 μl of 25% (w/w) $PLGA_{1000}$-PEG_{1000}-$PLGA_{1000}$ or $PLGA_{900}$-PEG_{1000}-$PLGA_{900}$) was determined by their incubation in the presence of 5.0 ml EPCs cell culture media (see below) in 24 well plates, in a humidified 5.0% CO_2 incubator at 37 °C for 10, 20, and 30 days. Following the incubation periods, the cell culture media was removed and the remaining hydrogels were washed with distilled H_2O several times and dried under vacuum up to a constant weight. The obtained dried polymer residuals were dissolved in $CDCl_3$ and characterized by ^1H NMR spectroscopy. The hydrogels degradation was also followed by phase contrast microscopy (Carl Zeiss Teraval 3) equipped with a DCM 300 digital camera (Hangzhou Huaxin IC Technology Inc., China).

4.5 Preparation and surface modification of nanodiamond films for implants functionalization

The ultrananocrystalline diamond (UNCD) coatings discussed in this chapter were grown by microwave plasma chemical vapour deposition (MWCVD) from gas mixtures containing 17% CH_4 in N_2. The substrate temperature was kept 600 °C, the working pressure 2.2 kPa, the microwave power 800 W, the deposition time 360 min. Detailed description of the MWCVD set-up is given in (Popov et al., 2006b). Monocrystalline silicon wafers were used as substrates which were ultrasonically pretreated in a suspension of diamond powders with different fractions in n-pentane prior the deposition in order to enhance the diamond nucleation on the surface. Such coatings were prepared also on a number of other materials of biomedical interest, for example, Ti-alloy used for implants (Kulisch & Popov, 2006).

In order to tailor the surface properties of the UNCD films with respect to their wettability, surface conductivity, etc., they were subjected to a number of surface modification processes as follows: i) H_2 microwave plasma at 400 °C in the deposition set-up (in the following: *HP*); ii) O_2 microwave plasma at room temperature (*OP*); iii) CHF_3 plasma in a 13.56 MHz parallel plate reactor also at room temperature (*FP*); iv) NH_3/N_2 plasma in a 13.56 MHz plasma enhanced chemical vapour deposition set-up at room temperature (*NP*); v) UV/O_3 photochemical treatment at room temperature (*UV*) and vi) chemical treatment with aqua regia (HCl/HNO_3 with a ratio of 3:1) at room temperature (*AR*). Further experimental details can be found in several references (Koch et al., 2011; Kulisch et al., 2010; Popov et al., 2008b).

4.6 Isolation and characterization of endothelial progenitor cells (EPCs)

Endothelial progenitor cells were isolated and cultured with minor modifications of the protocols described in earlier works (Fuchs et al., 2006a; Fuchs et al., 2006b). In brief, mononuclear cells were harvested from human peripheral blood buffy coats using Ficoll

(Sigma-Aldrich) gradient centrifugation and cultured in endothelial cell growth medium-2 (EGM-2 kit; CC-3162, Lonza, Belgium), 5.0% fetal calf serum (FCS; Lonza, Belgium), and 1.0% penicillin/streptomycin, on collagen-coated (BD Europe, Germany) well plates, where 5×10^6 cells per well were seeded. The good colonies of EPCs appeared after 3 to 4 weeks in culture. The EPCs' phenotype characterization was done following the protocol of (Fuchs et al., 2006a).

4.7 Transformation of EPCs to osteoblast

Two days after colony formation, the EPCs were trypsinized to single cells, passed through a 70 μm filter, and plated on 1.0 mm cover slips coated with hydrogels at 25 cells/cm^2 in osteoprogenitor medium (IMEM, Invitrogen) supplemented with 10% fetal bovine serum (Lonza, Belgium), 0.1 mM 2-mercaptoethanol, 2.0 mM Glutamax I, 2.0 mM BMP-2, and 0.2 mM ascorbic acid. The cultures were fed with osteoprogenitor medium every 2-3 days and allowed to differentiate up to 21 days to form mature bone nodules on different substrates. The transformation of endothelial phenotype of EPCs into long-term osteoblast culture growing on hydrogels or UNCD coatings was assessed as described previously (Popov et al., 2008a; Trajkovski et al., 2009) and followed by phase contrast and fluorescent microscopy, real time PCR (qPCR) and Western blot **(**Trajkovski et al., 2009**).** RNA and proteins were isolated with Trisol (Invitrogen, USA) following manufacturer's instruction on Day 1, 7, 14 and 21 after EPCs seeding on hydrogels and nanocomposites. Prior to amplification, the RNA purity and integrity were checked on Nanodrop-1000 (Termo-Scientific) and agarose gel electrophoresis. SYBR Green qPCR analysis was performed on RotorGene-6000 (Corbet) with the primers sequences and conditions as described by Woll et al (Woll et al., 2006; Woll & Bronson, 2006).

4.8 *In vivo* experiments

This study was carried out in accordance with the guidelines of the Medical University Pleven Ethics Committee (N 20/21.12.2010). A total of 24 adult female Wistar rats (220– 250 g, 3 animals per group) were used. Following i. p. injection of 45 mg/kg b.wt. ketamine a sterile 25% (w/w) $PLGA_{1000}$-PEG_{1000}-$PLGA_{1000}$ polymers with or without lovastatin (825 μM) or nanodiamonds (500 μg/ml) were implanted s. c. The animals were sacrificed on day 1 and 30 days later, and the explants were taken for further analysis.

4.9 Statistical analysis

The data were evaluated by analysis of variance (ANOVA) followed by Tukey's post-hoc test. Differences in the results at the level of $p<0.05$ were considered statistically significant. The statistical analysis was carried out using the PASW 18.0 statistical software package (IBM) for Windows.

5. Results

The structure-function properties of the native bone tissue pose strong design criteria to the substrates required to engineer their living counterparts or to be used in endogenous repair. When designing these substrates one should consider the macroscopic (organ level, geometry), the microscopic (cell and tissue level, scaffold architecture), and molecular properties relevant for tissue morphogenesis and function (e.g. hematopoiesis). In addition,

developmental aspects, such as growth, differentiation, migration and maturation should be taken into account, as these may dictate substrate properties, like degradation and porosity, or require additional instrumentation of bioactive factors (Bouten et al., 2011). Such scaffolds with a possible application for *in bone injection* have to be designed and studied very carefully, because the progenitor cells derived from bone marrow may also be homed on to the bioactive substrate.

5.1 Characterization of three-dimensional (3D) scaffolds

The composition of PLGA-PEG-PLGA block copolymers and its average molecular weight (M_n) were determined by ^{1}H NMR spectroscopy (Fig. 2). The broad chemical shift signal at 3.65 ppm marked as **b** is a characteristic of the methylene protons of the ethylene oxide repeating units. The signals observed at 1.58 ppm (signal **a**) CH_3-CH-, 5.2 ppm (signal **d**) CH_3-CH-, and 4.8 ppm (signal **c**) -O-CH_2-C(O)- are assigned to protons of methyl, methine, and methylene groups in lactide and glycolide units, respectively. The integrations (I_a, I_b, I_c, I_d) of the signals observed at 1.58, 3.65, 4.8 and 5.2 ppm assigned above were used for calculation of average molecular weight of all block copolymers following the equations:

$$M_{n\,(NMR)} = [(I_a/3)M_{Lac} + (I_c/2)M_{Gly} + M_{EO}] \times 4I_bDP_{PEG} \quad (1)$$

or

$$M_{n\,(NMR)} = [(I_dM_{Lac} + (I_c/2)M_{Gly} + M_{EO}] \times 4I_bDP_{PEG} \quad (2)$$

The DP_{PEG} is the degree of polymerization of the PEG block and $M_{Lac,}$ M_{Gly} and M_{EO} are the molecular weights, of the lactic, glycolic, and ethylene oxide segments. The calculated values of the average molecular weight of the block copolymers are represented in Table 2.

Sample	M_n, *(Theor.)*	M_n, *(NMR)*	M_n, *(GPC)*	M_w/M_n , *(GPC)*
$PLGA_{1000}$-PEG_{1000}-$PLGA_{1000}$	*3000*	*3150±122*	*3300±169*	*1.25*
$PLGA_{900}$-PEG_{1000}-$PLGA_{900}$	*2800*	*2948±151*	*3140±115*	*1.17*
$PLGA_{800}$-PEG_{1000}-$PLGA_{800}$	*2600*	*2873±177*	*2700*	*1.11*
$PLGA_{700}$-PEG_{1000}-$PLGA_{700}$	*2400*	*2664±113*	*2621*	*1.21*

Table 2. Characteristics of the PLGA-PEG-PLGA triblock copolymers. Data are representative from twelve independent syntheses and are expressed as average ± S.D.

The results showed deviations between the theoretically expected and the experimentally calculated molecular masses of all polymers. These deviations could be attributed to the presence of some moisture in the organic substances – monomers and PEG oligomer. The NMR data and those obtained from the GPC analysis reveal similar values for the molecular weight of all polymers. The received dispersity (M_w/M_n) indicates the narrow molecular weight distribution(see Table 2), which is typical for polymers prepared by a "living", controlled polymerization.

The composition of the polymers was also proved by FTIR spectroscopy. The spectra of all polymers show similar bands and signals. Only slight differences in the intensity of the bands attributed to the ester and ether type bonds at 1760 and 1163 cm^{-1} were observed and referred to the differences between the numbers of monomer units included in the polymer chains (data not shown).

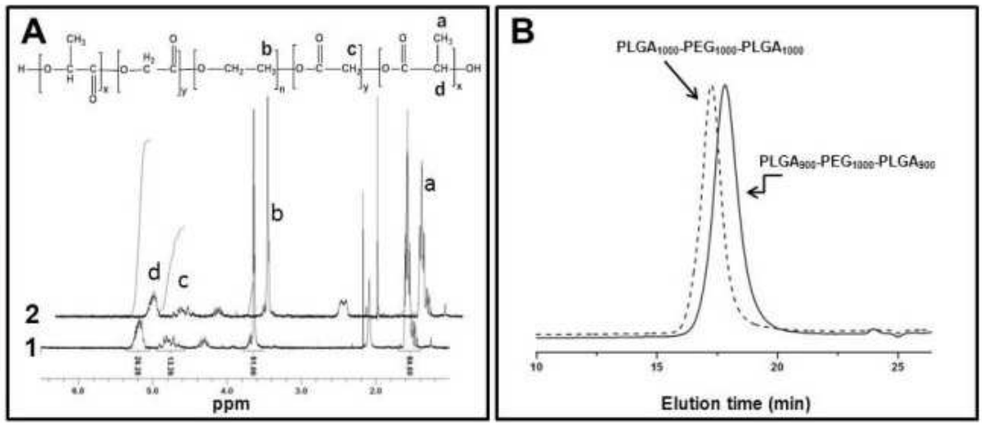

Fig. 2. Chemical characterization of the polymers. A: ^{1}H NMR spectra of $PLGA_{1000}$-PEG_{1000}-$PLGA_{1000}$ (1) and $PLGA_{900}$-PEG_{1000}-$PLGA_{900}$ (2) block copolymers; B: Molecular weight distribution overlay patterns of indicated polymers received by gel-permeation chromatography.

The copolymers with an analogous structure but a different ratio between the hydrophilic (PEG) and hydrophobic (PLGA) blocks have been an object of considerable scientific interest and value. The influence of the hydrophilic/hydrophobic ratio between PEG and PLGA blocks, and of the block length on the sol-gel–sol transition properties of PLGA-PEG-PLGA triblock copolymers has been reported (Lee et al., 2001). The authors have also found that the effects of different intramolecular/micellar behavior are accompanied by drastic changes in the area of gel zone.

5.2 Temperature–induced sol-gel phase transition of PLGA-PEG-PLGA block copolymers

In our work we chose to investigate PLGA-PEG-PLGA copolymers with much lower hydrophobic PLGA content (PEG:PLGA = 1:2 ; 1:1.8). The advantages of such hydrogels and especially their ability to be loaded with bioactive substances, drugs, cells, nanoparticles and etc., prior administration are of particular interests. The phase behavior (reversible sol-gel-sol transitions) of the obtained block copolymers in aqueous media at different temperatures and concentrations are illustrated in Fig. 3. As shown, only $PLGA_{1000}$-PEG_{1000}-$PLGA_{1000}$ and $PLGA_{900}$-PEG_{1000}-$PLGA_{900}$ copolymers possessed the typical gel-sol phase transition behavior upon heating. They have the ability to form temperature dependent micellar aggregates and after further temperature increase form gels due to micelles aggregation and/or packing. In contrast, the other two copolymers showed a vastly different performance. As the longer PLGA chains are present, stronger hydrophobic interactions are detected, leading to an increase in the aggregation and packing between the polymer micelles resulting in the formation of a denser gel state. The gel zone in the phase diagram of $PLGA_{800}$-PEG_{1000}-$PLGA_{800}$ and $PLGA_{700}$-PEG_{1000}-$PLGA_{700}$ copolymers was not found. Nevertheless, we observed significant alterations of their viscous properties – changes from amber viscous to white viscous state. With additional rise of the temperature, direct transition from white viscous to suspension state was also observed. The slight increase in the temperature enhances the thermal motion of the hydrophobic chains in the $PLGA_{800}$-PEG_{1000}-$PLGA_{800}$ and $PLGA_{700}$-PEG_{1000}-$PLGA_{700}$ copolymers, which may lead to the disturbance of the micellar structures and polymer precipitation.

Injectable biodegradable copolymer hydrogels, which exhibit a sol–gel phase transition in response to external stimuli, such as temperature changes, have found several biomedical and pharmaceutical applications, such as drug delivery, cell growth, and tissue engineering (Gao et al., 2010; Kan et al., 2005; Kim et al., 2001; Nguyen & Lee, 2010; Qiao et al., 2006; Zentner et al., 2001). Such polymers are also biocompatible and biodegradable, and they represent an ideal system for treatment, being able to overcome the problem of carrier removal after injection (implantation). Hydrogels sensitive to temperature are useful for both *in vitro* and *in vivo* applications. These applications will strongly depend on hydrogels composition and it is important to administer the sol dispersion upon quick transformation to gel under physiological conditions. The composition, morphology and crystallinity of the block copolymers strongly influence the mechanical properties and rate of degradation under specific conditions. To study the *in vitro* behavior of the $PLGA_{1000}$-PEG_{1000}-$PLGA_{1000}$ and $PLGA_{900}$-PEG_{1000}-$PLGA_{900}$ copolymers we used light microscopy and ^1H NMR spectroscopy.

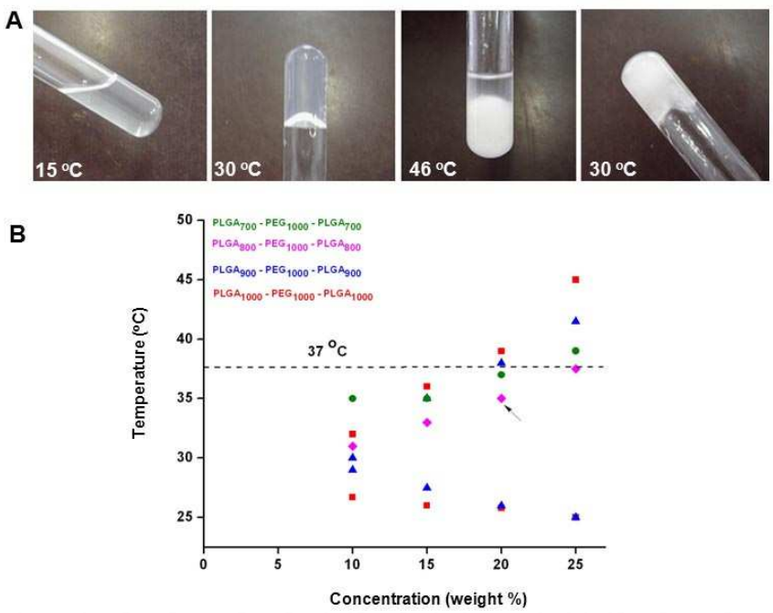

Fig. 3. Sol-gel transitions of $PLGA_{1000}$-PEG_{1000}-$PLGA_{1000}$ block copolymer (A) and phase diagrams of PLGA-PEG-PLGA triblock copolymers (B).

5.3 *In vitro* degradation of the polymeric hydrogels

Polymer degradation is the key process of erosion and plays a crucial role for all polymers studied. The processes involved in the erosion of a degradable polymer are very complicated. They can be summarized as follows: (1) water enters the polymer bulk; (2) water entrance may be accompanied by swelling; (3) chemical polymer degradation appears, leading to the creation of oligomers and monomers.; (4) the degradation changes the microstructure of the hydrogels through pore formation; (5) oligomers and monomers are released; (6) dissolution and diffusion of oligomers and monomers are undergoing; (7) the pH inside the pores can be changed, depending of polymer composition; (8) finally, the released oligomers and monomers lead to the weight loss of the hydrogels.

Fig. 4 reflects the hydrogels morphology after 10 and 30 days in contact with 5.0 ml EPC culture media at 37 °C. The 20 and 25% (w/w) $PLGA_{1000}$-PEG_{1000}-$PLGA_{1000}$ and $PLGA_{900}$-PEG_{1000}-$PLGA_{900}$ copolymer samples were about 1.0 mm thick and 1.0 cm in diameter.

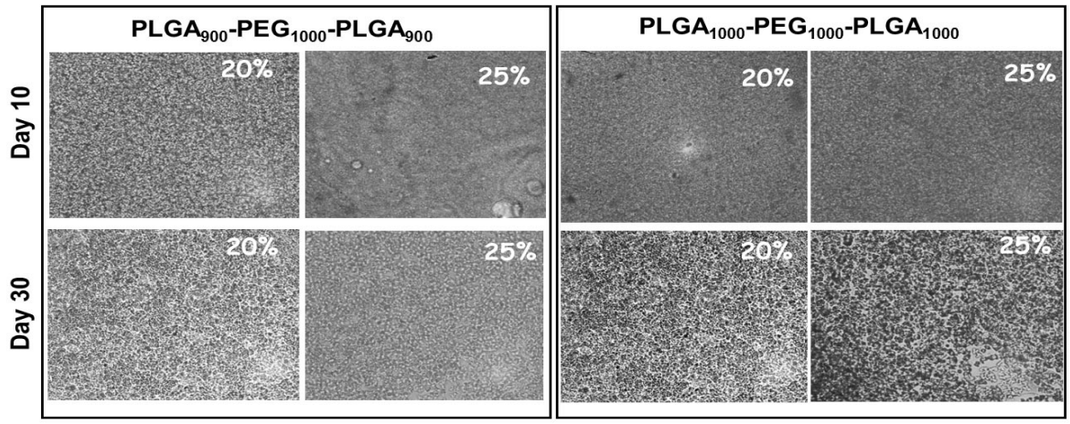

Fig. 4. Optical microscopic images of the polymeric hydrogels during their destruction in cell culture environment. Magnification: x100.

Changes in the weight-average molecular weight (M_W) of PEG and PLGA components in the scaffolds as a function of degradation time are shown in Fig. 5. It can be seen that the M_W of hydrogels decreased with incubation time for all of the scaffolds. There were no significant differences in the degradation rate between 20 and 25% hydrogels. The decrease in molecular weight can be attributed to hydrolysis and macromolecular scission of PLGA (Shih et al., 1996). Monomer release profiles for PLGA have a short induction period. The release rate was higher at early times and declines in a concave manner.

The acidic degradation products of PLGA did not lead to severe decrease in the pH values. It drops from 7.4 (Day 1) to 6.4 (Day 30). To evaluate the degradation of the scaffolds, the medium pH for the specimens was compared to media that was held under the same conditions but did not contain any samples (blank). The EPC's media with a lower pH than the blank one would indicate the release of acidic products from the scaffolds and can lead to faster degradation.

By 24 h the difference between the blank media pH and the pH of the media in contact with hydrogels was negligible and remained so through 1 week. On day 10, the pH of the media incubated with hydrogels began to decrease. This decrease in pH persisted through week 2 and 3, with a maximum deviation from blank pH of - 0.94 ± 0.06 at week 4.

It was noticed that the weight loss was about 39% after 30 days degradation in the cell culture media, however, it was 30% just after 10 days. We used the formulas (1) and (2) mentioned above to calculate the changes in the hydrogels' molecular weight - molar content of the different co-compounds. It should also be kept in mind, that the obtained values are relative and don't represent actual PLGA and PEG content in the hydrogels or overall molecular weight of the polymeric chains, but can be used for the construction of a simple qualitative model describing their destruction. Looking at Fig. 5 we can see significant changes or decreasing in the content of PEG part in hydrogels i. e. decreasing the molecular weight of the corresponding copolymers with the time. Similar indicated changes in the hydrophobicity of the polymeric materials of similar type have also been reported by (Youxin et al., 1994; Zweers et al., 2004).

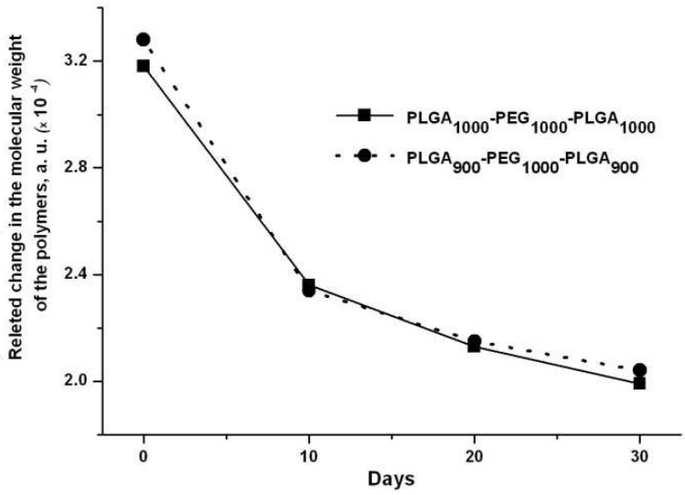

Fig. 5. The relative change in the composition of the block copolymers with the time. Alteration in the molecular weight of PLGA are calculated at a constant PEG content and molecular weight.

The mechanism of erosion/degradation of the polymeric hydrogels can be presented by the general scheme shown in Fig. 6. It can be summarized as follow: (1) the amphiphilic PLGA-PEG-PLGA three-block copolymers form stable micelle solutions; (2) under the influence of thermal fluctuations on the polymeric chains, the micelles are packed into a crystalline-like structure – hydrogel; (3) the H_2O immerges into hydrogels, and the quick swelling happens; (4) when the swelling equilibrium is reached, the chains start to break as a function of time; (5) the presence of water provokes bulk degradation of the hydrogels via a random hydrolytic scission of the ester linkages in the vicinity of PEG; (6) sustained release of water-soluble PEG and PEG's end-capped with short PLGA tails; (7) the hydrophobicity of the remaining hydrogel should increase; (8) as the experiments were conducted in cell culture media with high buffer capacity, the further hydrolysis of glycolic–glycolic and glycolic–lactic ester bonds by lactic and glycolic acids will be slow down.

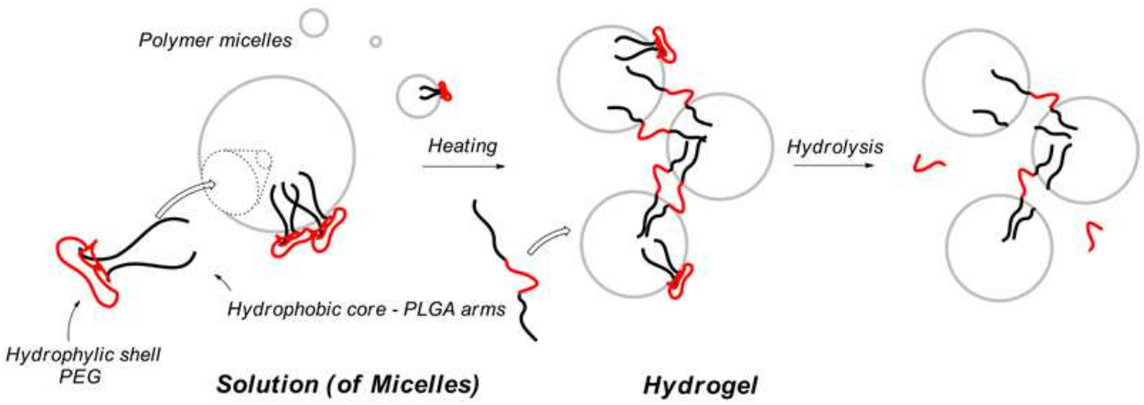

Fig. 6. Schematic representation of hydrogel formation and erosion/degradation.

Sol-gel transition characteristics, including transition temperature and gel window width are the critical parameters which should be taken into consideration in designing 3D

scaffold biomaterials. For *in vitro* and *in vivo* application is also necessary to know their behavior in surrounding environments. To follow the biochemical and molecular biological response of the composites prepared by us we investigated the possibility these polymers to be prepared as a cell loaded form.

5.4 Scaffold colonization and seeding efficiency

The EPCs' attachment and differentiation were performed on sample scaffolds prepared with or without NCDs and lovastatin to evaluate the cell biocompatibility. The experiments suggested that on day 1 of culturing low number of cells was attached to all scaffolds studied. The loading efficiency reached 73.1 ± 5.3% after 3 days on PLGA-PEG-PLGA + NCDs and composites with NCDs and lovastatin (89.6 ± 5.7%) and only 11.4 ± 1.5% for the PLGA-PEG-PLGA + lovastatin. A qualitative analysis of cell adhesion on the scaffolds was carried out by phase contrast microscopy up to 21 days. This study (Fig. 7) demonstrated that the cells were distributed unequally throughout the surface structure with different morphology at the beginning. The results presented in Fig. 7 also confirmed the infiltration and migration of cells deep into the 3D porous network on scaffolds containing NCDs or NCDs + lovastatin only. Cells with distinct rounded nuclei were observed throughout the scaffold, further suggesting normal cell growth on these composites. The results about EPCs adhesion on PLGA-PEG-PLGA scaffolds can found in (Trajkovski et al., 2009; Ivanova et al., 2011).

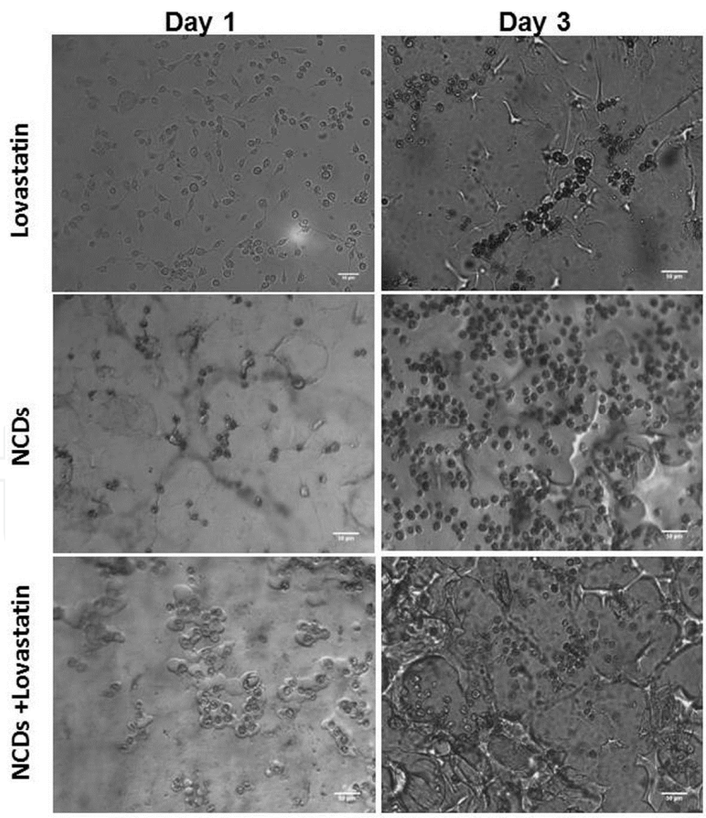

Fig. 7. Endothelial progenitor cells growing on different type composites based on 25% (w/w) $PLGA_{1000}$-PEG_{1000}-$PLGA_{1000}$ hydrogel, containing lovastatin and/or nanocrystalline diamonds (NCDs). Bars 50 μm.

Next we have examined the release of fibronectin (FN) during the EPCs differentiation to osteoblast. Fluorescent photomicrographs of FN stained cells are shown on Fig. 8. As it can be seen the cell response is heterogeneous and FN distributes in a diffuse, punctate pattern of staining throughout the whole surface. The obtained results can be summarized as follows: (1) FN release was detected on day 7 and this was connected with its adsorption to the surfaces; (2) During the process of EPCs differentiation, the release of FN was favored by the hydrogels + NCDs (day 12, 15, and 21). These observations confirmed the hypothesis suggesting that FN is adsorbed preferentially on hydrophobic surfaces (Nordahl et al., 1995), such as the surface of the hydrogels + NCD undergoing erosion. It has also been suggested that FN plays a unique role during the differentiation of osteoblast cultures connected with the formation of mineralized nodules *in vitro* (Robey, 1996). We have reported results confirming this observation (Ivanova et al., 2011).

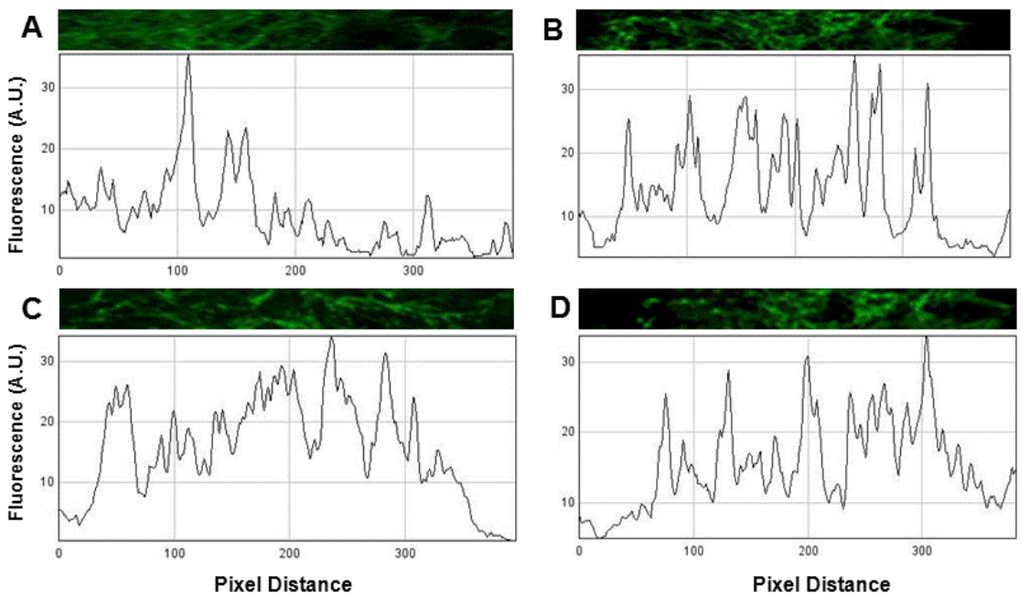

Fig. 8. Composite induced changes in distribution of fibronectin. Hydrogels were based on 25% $_{(w/w)}$ $PLGA_{1000}$-PEG_{1000}-$PLGA_{1000}$ (A); $PLGA_{1000}$-PEG_{1000}-$PLGA_{1000}$ + lovastatin (B); $PLGA_{1000}$-PEG_{1000}-$PLGA_{1000}$ +nanocrystalline diamonds (C); $PLGA_{1000}$-PEG_{1000}-$PLGA_{1000}$ + lovastatin + nanocrystalline diamonds (D). The tracings immediately under each panel are scans of the pixelated fluorescence intensity of fibronectin integrated vertically and scanned horizontally across the magnified field.

All data obtained by us indicated that not only the PLGA-PEG-PLGA scaffolds are biocompatible with the EPCs as reported (Trajkovski et al., 2009; Ivanova et al., 2011), but composites with NCDs actually promote their growth and transformation. The processes of EPCs differentiation can influence the expression of several important genes. We further followed these changes by quantitative real time PCR analyses.

5.5 qPCR analysis of mRNA derived from endothelial progenitors cells undergoing transformation to osteoblasts

The expression of four osteogenic markers *Twist1, Runx2, Osterix,* and *Bglap1*, and the endothelial one - platelet endothelial cell adhesion molecule (*PECAM1)*, was analyzed at

various time points throughout the transformation of the EPCs culture to osteoblasts. The results shown on Fig. 9 revealed a gene expression pattern characteristic of the osteoblast differentiation. The expression of *Twist1 and Osterix* was highly upregulated by day 14 and persisted to day 21 without significant differences between scaffolds studied. *Runx2* and *Bgalp1* expression was continuously increasing during the differentiation and it was found to be significantly higher (Day 7: p=0.034; Day14: p=0.011; Day 21: p=0.07) in EPCs growing on composite scaffolds containing NCDs in comparison with hydrogels ± lovastatin. The PECAM-1 was expressed at the beginning of the differentiation process, but decreased on days 7 and 21. Incorporation of the lovastatin in hydrogels increased the expression of PECAM-1 at day 7 about five times.

In comparison to the hydrogels ± lovastatin, the scaffolds ± NCDs leaded to upregulation of the osteoblasts associated markers at two time points of investigation (Day 7 and 21). In accordance with these observations the total protein amount of Runx2, Osteocalcin and Collagen-α1 was also high (Trajkovski et al., 2009). *Runx2 mRNA* and protein amount were found to increase continuously. Their expression is also critical for mature osteoblast function. RUNX2 binding sites were identified in the osteoblast specific genes encoding osteocalcin, bone sialoprotein, and osteopontin, as well as type I collagen (Ducy et al., 1997). The detected earlier expression of *Runx2 mRNA* might positively influence the latter expression of osteocalcin and collagen-α1 observed by us. The registered increase in *PECAM1 mRNA* demonstrated at Day 1 and 7 also showed the ability of EPCs to switch the differentiation process under specific conditions and confirmed that the lovastatin can stimulate the PECAM-1 expression in endothelial cells. The gene expression data provide strong evidence for osteogenic transformation of the EPCs to osteoblasts on all scaffolds tested.

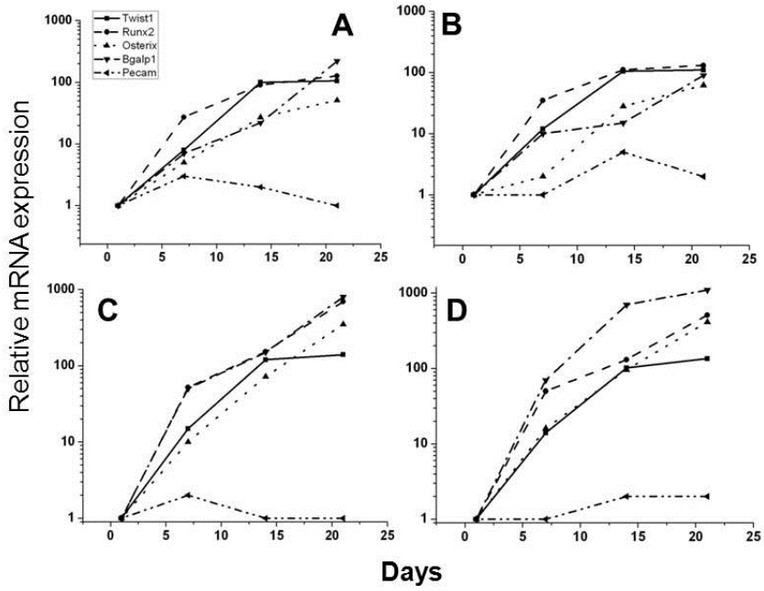

Fig. 9. Quantitative PCR analysis of endothelial progenitor cells (EPCs) undergoing differentiation to osteoblasts. EPCs growing on 25% $_{(w/w)}$ $PLGA_{1000}$-PEG_{1000}-$PLGA_{1000}$ (A); $PLGA_{1000}$-PEG_{1000}-$PLGA_{1000}$ + lovastatin (B); $PLGA_{1000}$-PEG_{1000}-$PLGA_{1000}$ +nanocrystalline diamonds (C); $PLGA_{1000}$-PEG_{1000}-$PLGA_{1000}$ + lovastatin + nanocrystalline diamonds (D). Each assay was run in triplicate at three different template concentrations. Relative mRNA expression is normalized to ribosomal protein L7 (Rpl7), displayed relative to Day 1, and presented as a common log plot.

The tissue engineering is based on the method of cell seeding on scaffolds that play a role as a matrix to guide cell growth and to assist the formation of functional new tissues. Scaffolds grant this process by promoting an appropriate surface and sufficient spaces to favor the cell attachment, migration, proliferation and special differentiation in three dimensional ways. The design of the scaffold is the most important because it influences the above mentioned processes. There are many worldwide accepted criteria for ideal scaffolds with application in tissue engineering and the critical ones include the main material, mechanical properties, 3D architecture, surface morphology and chemistry, as well as the scaffold environment before and after the degradation process (Wei G. & Ma P.X., 2007). Other important properties are: (1) to be biocompatible – non-immunogenic and (2) non-toxic for the living cells and tissue. To test the biocompatibility of the scaffolds prepared by us we have conducted the *in vivo* experiments.

5.6 *In vivo* mass decrease of polymer hydrogels

The 3D-scaffolds loaded with lovastatin and/or nanodiamods and injected in rats provide an evidence for biocompatibility and degradability. To examine time-dependent *in vivo* mass loss of polymer hydrogels, we prepared sterile 25% (w/w) $PLGA_{1000}$-PEG_{1000}-$PLGA_{1000}$ ± NCDs ± lovastatin and injected them into the rats, subcutaneously. Injectable hydrogels for biomedical applications should be degraded or eliminated from the body after accomplishment of their role. Fig. 10 shows *in situ* gel formation of a polymer solution and separated gels explanted at 2 time points. All polymer solutions transformed to hydrogels, and the hydrogels showed time-dependent mass decrease behaviors.

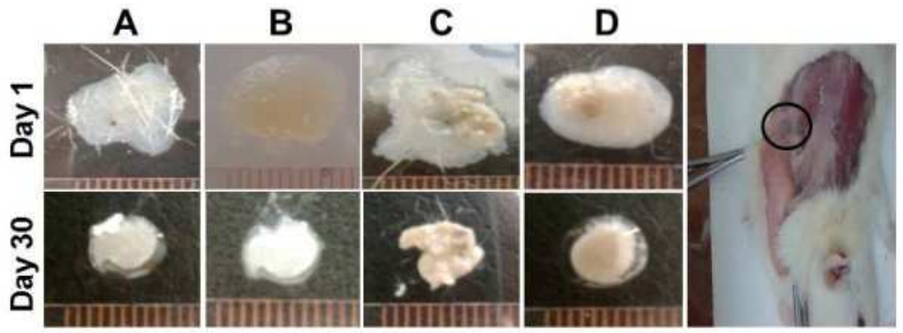

Fig. 10. *In vivo* time-dependent mass decrease of polymer hydrogels. Photographs of separated polymer explants and *in situ* gelation of the polymer solutions from s.c. injected rats. 25% $_{(w/w)}$ $PLGA_{1000}$-PEG_{1000}-$PLGA_{1000}$ (A); $PLGA_{1000}$-PEG_{1000}-$PLGA_{1000}$ + lovastatin (B); $PLGA_{1000}$-PEG_{1000}-$PLGA_{1000}$ +nanocrystalline diamonds (C); $PLGA_{1000}$-PEG_{1000}-$PLGA_{1000}$ + lovastatin + nanocrystalline diamonds (D).

The hydrogels containing $PLGA_{1000}$-PEG_{1000}-$PLGA_{1000}$ alone showed the fastest mass decrease, but they still remained detectable within 4 weeks. The mass of the polymer hydrogels was decreased in the order of $PLGA_{1000}$-PEG_{1000}-$PLGA_{1000}$ + NCDs ≅ $PLGA_{1000}$-PEG_{1000}-$PLGA_{1000}$ + lovastatin + NCDs > $PLGA_{1000}$-PEG_{1000}-$PLGA_{1000}$ + lovastatin > $PLGA_{1000}$-PEG_{1000}-$PLGA_{1000}$. After 4 weeks, the remained masses of hydrogels were 59%, 58%, 48 and 23%, respectively. We also noticed that around 3 of the $PLGA_{1000}$-PEG_{1000}-$PLGA_{1000}$ + lovastatin loaded hydrogels less capillaries were present, which can be attributed to the negative effect of lovastatin on endothelial cell proliferation and angiogenesis. It may also be connected with the difference of

environment, especially water content. There was no adverse effect during the *in vivo* tests. The observed results suggest that polymeric solutions ± NCDs and ± lovastatin can be used as injectable and biodegradable hydrogels and the degradation rate of the composites can be controlled by adjusting substituent compositions.
Since the scaffolds with NCDs showed very good biocompatibility the next step was to test the opportunity for preparation of new, bio-enhanced UNCD containing films with potential application for implant preparation.

5.7 ND film modifications and the role of implant functionalization

The UNCD films deposited under the conditions described above have been comprehensively characterized with respect to their crystallinity, composition, topography and bonding structure (Popov et al., 2003; Popov et al., 2004; Popov C. & Kulisch W., 2003). The X-ray diffraction and selected area electron diffraction (Fig. 11A) revealed patterns characteristic for diamond phase. Furthermore, the size of the diamond crystallites was determined from the XRD peaks to be on the order of 3-5 nm. These nanocrystallites are embedded in an amorphous carbon matrix with a grain boundary width of 1.0-1.5 nm, as shown by TEM (Popov et al., 2004). The ratio of the volume fractions of the two phases-crystalline and amorphous - estimated from the density of the coatings and from the total crystallinity is close to unity (Popov et al., 2003). Investigations of the UNCD films with Raman spectroscopy, X-ray photoelectron spectroscopy (XPS), electron energy loss spectroscopy (EELS, Fig. 11B) and Auger electron spectroscopy (AES) showed the presence of sp^2-bonded carbon atoms (up to 15 at%) localized in the amorphous matrix (Popov et al., 2003; Popov et al., 2004). Although no H_2 was added to the precursor gas mixture, the UNCD films contain about 9-10 at% H in the bulk, as revealed by elastic recoil detection (ERD) analysis, originating from the CH_4 molecules. Fourier transform infrared spectroscopy showed that hydrogen is bonded predominantly in sp^3-CH_x groups (Popov & Kulisch, 2003).

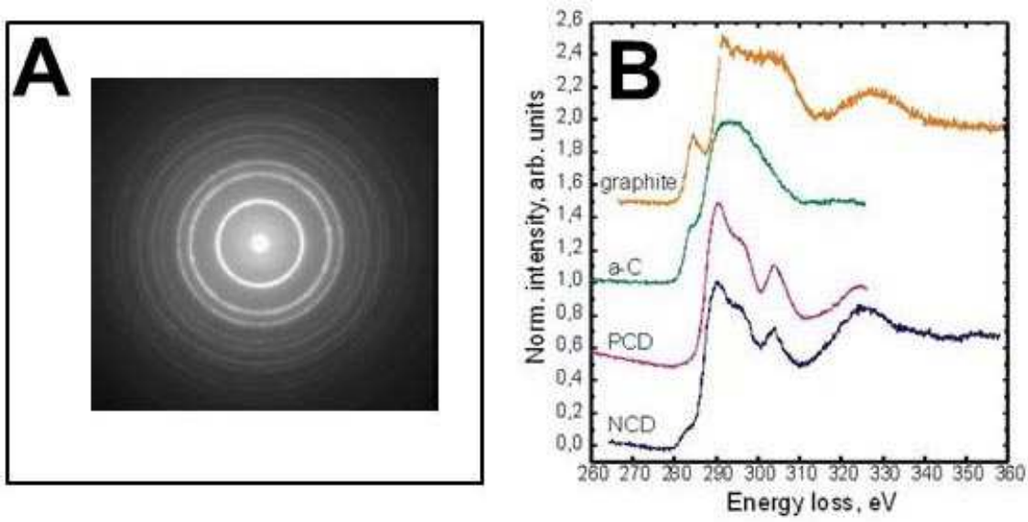

Fig. 11. Physico-chemical characterization of the UNCD films. (A) Selected area electron diffraction of UNCD film; (B) Electron energy loss spectra of different carbon materials (Popov et al., 2004; Popov et al., 2011).

Atomic force microscopy (AFM) studies showed for all investigated samples the characteristic topography of UNCD films, composed of structures with diameters of several hundred nanometers, which themselves possess a substructure (Fig. 12A). The root mean square surface roughness values lie in the narrow range of 10 – 14 nm (Kulisch et al., 2011). The nanostructured surface can expect to enhance the attachment of cells on it. The surface composition of the as-grown UNCD films (*AG* in the following) was investigated by XPS. The results showed that the as-grown surfaces are very clean, with oxygen and nitrogen concentrations of about 2.0 and 1.0 at%, respectively. Nuclear reaction analysis (NRA) revealed the depth profiles of hydrogen concentration in the UNCD films and indicated surface H concentration of 12-14 at% (Fig. 12B)(Kulisch et al., 2008).

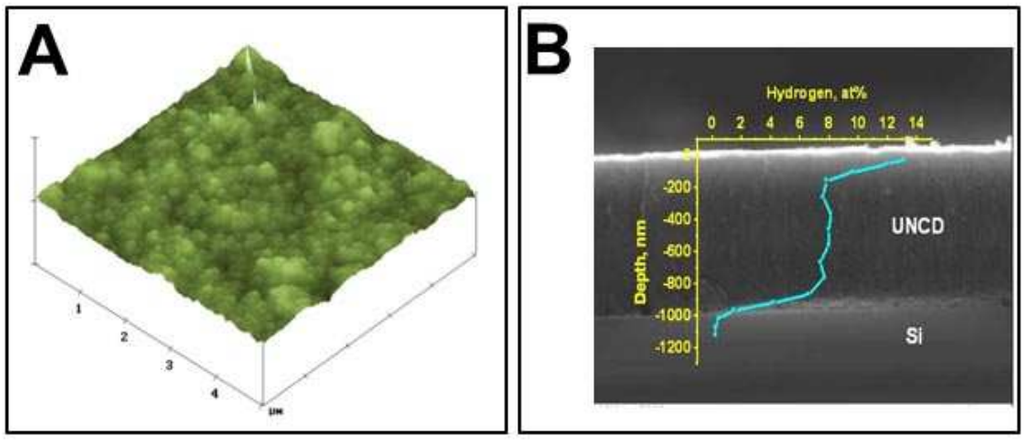

Fig. 12. AFM image of the surface of UNCD film revealing the typical topography of the coatings (A) and Hydrogen depth distribution determined by nuclear reaction analysis and scanning electron microscopy cross section micrograph of UNCD film (B) (Kulisch et al., 2008; Popov et al., 2003; Popov et al., 2011).

The surface composition of UNCD films after different modifications, described above, has been also investigated by XPS (Popov et al., 2008b) and the results are summarized in Fig. 13A. As already mentioned, the surface of *AG* is very clean, the same holds for *AR*. The sample *NP* exhibits an increase of the surface nitrogen concentration from 1.0 to 7.4 at% after ammonia treatment (Koch et al., 2011). It was found that the oxygen content of the O_2 plasma treated surface is about 12 at% (*OP*) and about 8.5 at% for the UV/O_3 treated sample (*UV*), in contrast to 2.0 at% for *AG*, indicating an oxidation of the surface by both processes. The plasma treatment with CHF_3 leads to a surface fluorine concentration of almost the same value (ca. 12 at%) showing that a fluorination process has taken place on the surface. Having in mind that the hydrogen surface concentration of the as-grown samples is about 14 at% (Kulisch et al., 2008), the XPS results indicate a change of the surface termination by the plasma processes. Closer analyses of the XPS peaks revealed that in the case of the oxygen plasma treatment the terminating hydrogen atoms are replaced by O and OH groups rather than by carboxylic acid groups (Popov et al., 2008b). CHF_3 plasma treatment has led to a substitution of the C-H bonds by C-F rather than to the deposition of a $C_xH_yF_z$ polymer (Popov et al., 2008b).
The wettability of the differently treated UNCD surfaces against purified water were examined by contact angles measurements. The results presented in Figs. 13B and 14 show

that all applied treatments have resulted in modification of the original surface. Three types of surfaces can be differentiated: hydrophobic (*AG*, *HP*, *FP*), hydrophilic (*OP*, *NP*, *UV*) and surface *AR* in between the two groups. The contact angles q_C of the three highly hydrophobic samples are in the order *AG* < *HP* < *FP* varying between 85 and 100°, while all hydrophilic samples possess q_C < 10°. The contact angle of *AR* is 67° showing also a hydrophobic character.

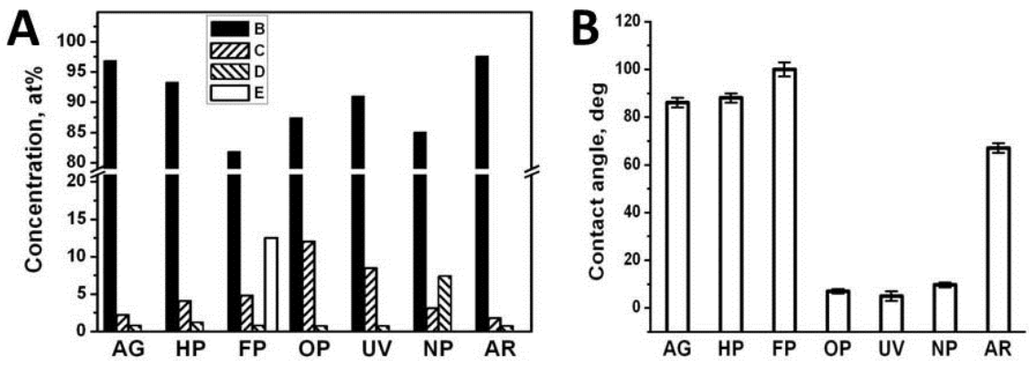

Fig. 13. Surface composition of ultananocrystalline diamond/amorphous carbon composite films after different treatments (B – carbon; C- oxygen; D- nitrogen; E- fluorine) (A) and contact angles of same surfaces after different treatments (B) (Popov et al., 2011).

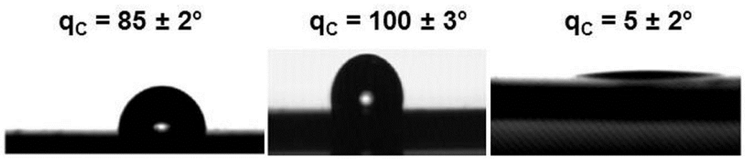

Fig. 14. Contact angles and water droplet profiles on ultananocrystalline diamond/amorphous carbon composite films: as-grown (left), after F-containing plasma modification (middle) and after UV/O_3 treatment (right) (Popov et al., 2011).

The interaction of a surface with cells is usually dominated (at least in the initial stage) by adhesion of proteins onto the biomaterial surface, which occurs rather rapidly. For this reason it is important to study the interactions of proteins with UNCD surfaces and to tailor them, if necessary, by suitable surface modifications. Up to now, three series of experiments have been carried out to investigate the UNCD/protein interactions.

In the first series, scanning force spectroscopy measurements have been performed with as-grown UNCD films and glass (as a reference) onto which proteins have been deposited. A silicon cantilever functionalized with bovine serum albumin (BSA) has been used for this purpose. 120 single measurements at different positions have been performed for each of the two samples. On the UNCD sample none of 120 measurements indicated any interaction; all force curves had the structureless shape. In contrast, for the glass sample in 38% of all force/distance measurements an interaction between the BSA-functionalized cantilever and the surface was observed, which gave rise to force curves. Thus it can be concluded that the UNCD surfaces are not prone to unspecific interactions with proteins (Popov et al., 2007).

On the other hand, even on such inactive surfaces there will be adhesion of highly fouling proteins such as BSA. In order to investigate whether the BSA adhesion on UNCD films is influenced by the surface termination, several of the above discussed surfaces have been

subjected to BSA exposure in the second series of experiments. Immediately after this exposure the surfaces were investigated by time of flight secondary ion mass spectroscopy (ToF-SIMS) and XPS (Kulisch et al., 2007). According to the ToF-SIMS analysis, all surfaces were covered by a BSA layer approaching a monolayer but it turned out to be impossible to quantify the adhesion and to evaluate differences between the various surfaces. More insight into this question was brought by XPS measurements. The surface composition of all samples investigated was far from that of a thick spin-coated BSA layer on a silicon substrate, taken as a reference, indicating that the BSA coverage on the UNCD surfaces is limited. As the composition of the starting surfaces is different as discussed above, it seems to be more useful to look at the compositional changes inferred by the BSA exposure which are shown in Fig. 15A. From this figure it is evident that the changes of the surface composition of the as-grown *AG* surface are only marginal. They are more pronounced for the H_2 and O_2 plasma treated samples (*HP* and *OP*). The largest changes, and thus the highest adhesion of BSA, were observed for the chemically aqua regia treated surface *AR*. A possible reason is the partial loss of the hydrogen termination caused by the treatment as discussed above. Summarizing, it can be stated that the unspecific adhesion of biomolecules such as the highly fouling bovine serum albumin on UNCD surfaces can be influenced by the surface termination.

In the third series of experiments, the protein adsorption on UNCD surfaces with different terminations was studied by inverted enzyme-linked immunosorbent assay (ELISA) with albumin and fibrinogen (Popov et al., 2009). The ratio of albumin to fibrinogen adsorption was calculated from the individual levels of both proteins adsorbed on the surfaces (Fig. 15B). The oxygen terminated layers exhibit a higher albumin to fibrinogen ratio as compared with the fluorine and hydrogen terminated films. It has been pointed out that the variation of the albumin and fibrinogen adsorption ratio is strongly related to the associated surface energies since fibrinogen, being itself hydrophobic, preferentially adsorbs on hydrophobic surfaces, but albumin (with a hydrophilic nature) on hydrophilic surfaces during competitive binding. The O-terminated UNCD layers have a hydrophilic surface (33° contact angle against water), leading to a higher albumin/fibrinogen ratio. The F-terminated films show the lowest protein ratio, which is related to the hydrophobic nature of these surfaces (contact angle of water 91°). Therefore the albumin adsorption is much greater on the oxygen terminated surfaces and vice versa – the fibrinogen is preferentially adsorbed on the hydrophobic fluorine and hydrogen terminated surfaces.

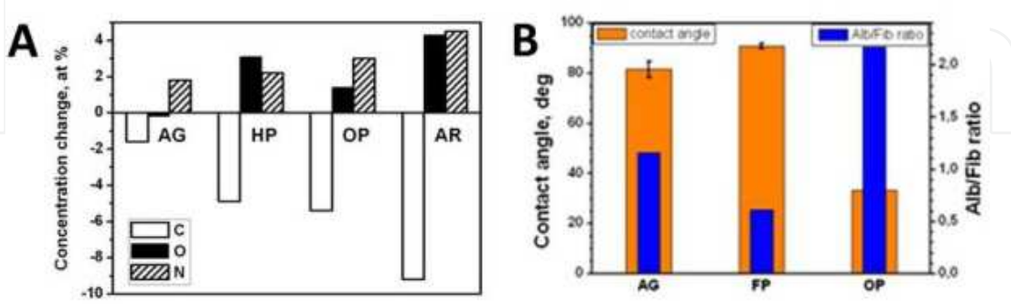

Fig. 15. Relative changes of the surface composition caused by the exposure of the samples to bovine serum albumin (A) and Contact angles and BSA/fibrinogen adsorption ratios on differently terminated UNCD surfaces (B) (Popov et al., 2011).

The biocompatibility of UNCD films was studied by direct contact tests with osteoblast-like cells, fibroblasts and endothelia cells (Popov et al., 2006a; Popov et al., 2007; Popov et al.,

2008a). All cells showed good adhesion and spreading on the UNCD surfaces following the incubation. After several days of cultivation they formed confluent monolayers; comparisons with cells from control samples showed that the UNCD films are not cytotoxic and do not affect the cell viability and proliferation.The coatings are also bioinert as revealed by simulated body fluid (SBF) tests. The exposure to SFB with a composition close to that of blood plasma for 10 days did not result in the formation of hydroxyapatite as shown by analyses of the SBF composition and of the film surface (Popov et al., 2006a).

6. A look at the future

Extraordinary progress has been made in the last decade towards the design of implants and scaffolds with a suitable multi-scale hierarchical structure. The limitations of the design of current bone implants arise mainly from the lack of firm quantitative mechanical data of bones in different stages of osteoporosis. Whilst it is known that osteoporotic bone is generally not cancellous in nature and has thin walls, the essential design paradigm of implants does not reflect this application.

A simple system for assisted bone repair proposed is the *in bone injection* of "intelligent" polymers combined with progenitor cells. It utilizes autologous stem cells transplantation in combination with supportive bioresorbable matrices and bioactive molecules for enhancing growth and repair. Ideally, endothelial progenitor cells obtained from peripheral blood of the same patient may be cultured *in vitro* in the presence of different stimuli and/or nanoparticles to undergo osteoblasts differentiation, prior to autologous transplantation. This injectable therapy could also be used for: (1) modifying the bone interior morphology, porosity and interconnectivity, which are extremely important for cell adhesion, proliferation and differentiation; (2) prophylactic treatment for high risk patients to prevent fractures, especially the hip and vertebrae; (3) treatment to stabilize loose prostheses for patients who would soon require revision surgery; (4) providing exceptional repair of the osteoporotic bone by releasing pharmaceuticals to the specific sites with the purpose of accelerating healing, promoting angiogenesis, reducing the risk of infection, etc.

The pursuit of effective treatments for osteoporotic disease is an extremely challenging scientific frontier requiring the integration of multiple engineering, biological, chemical, surgical, and pathophysiology related disciplines. It is also necessary to have a better understanding of molecular and cellular mechanisms specific to osteoporosis. Studying genomics, proteomics and diseases biology in parallel is likely to yield transformative insights in this regard. Our results together with the continuously incoming new data could have direct implications in the use of biomaterials in tissue engineering and in combination with the rapid manufacturing techniques will offer great opportunities to generate different scaffolds for bone engineering in near future.

7. Acknowledgment

We are grateful to the National Science Fund of Bulgaria (Grant TKX-1704) for their financial support.

8. Conflict of interest

This book chapter has been published with the financial support of the "Human Resources Development" Operational Programme, co-financed by the European Union through the

European Social Fund. The whole responsibility for the data contents lies with the Beneficiary and under no circumstances should this collection be regarded as representing the official position of the European Union and the Contract Body.

9. References

Aitman, T. J.; Dong, R.; Vyse, T. J.; Norsworthy, P. J.; Johnson, M. D.; Smith, J.; Mangion, J.; Roberton-Lowe, C.; Marshall, A. J.; Petretto, E.; Hodges, M. D.; Bhangal, G.; Patel, S. G.; Sheehan-Rooney, K.; Duda, M.; Cook, P. R.; Evans, D. J.; Domin, J.; Flint, J.; Boyle, J. J.; Pusey, C. D. & Cook,H.T. (2006). Copy number polymorphism in Fcgr3 predisposes to glomerulonephritis in rats and humans. *Nature*, Vol.439, No.7078, pp. 851-855

Annefeld, M.; Caviezel, R.; Schacht, E. & Schicketanz, K. H. (1986). The influence of ossein-hydroxyapatite compound ('Ossopan') on the healing of a bone defect. *Curr. Med. Res. Opin.*, Vol.10, No.4, pp. 241-250

Bloemers, F. W.; Blokhuis, T. J.; Patka, P.; Bakker, F. C.; Wippermann, B. W. & Haarman, H. J. T. M. (2003). Autologous bone versus calcium-phosphate ceramics in treatment of experimental bone defects. *Journal of Biomedical Materials Research Part B-Applied Biomaterials*, Vol.66B, No.2, pp. 526-531, ISSN/ISBN 0021-9304

Bouten, C. V.; Dankers, P. Y.; Driessen-Mol, A.; Pedron, S.; Brizard, A. M. & Baaijens, F. P. (2011). Substrates for cardiovascular tissue engineering. *Adv.Drug Deliv.Rev.*, Vol.63, No.4-5, pp. 221-241

Cappuzzo, F.; Hirsch, F. R.; Rossi, E.; Bartolini, S.; Ceresoli, G. L.; Bemis, L.; Haney, J.; Witta, S.; Danenberg, K.; Domenichini, I.; Ludovini, V.; Magrini, E.; Gregorc, V.; Doglioni, C.; Sidoni, A.; Tonato, M.; Franklin, W. A.; Crino, L.; Bunn, P. A., Jr. & Varella-Garcia,M. (2005). Epidermal growth factor receptor gene and protein and gefitinib sensitivity in non-small-cell lung cancer. *J.Natl.Cancer Inst.*, Vol.97, No.9, pp. 643-655

Conrad, D. F.; Andrews, T. D.; Carter, N. P.; Hurles, M. E. & Pritchard, J. K. (2006). A high-resolution survey of deletion polymorphism in the human genome. *Nat.Genet.*, Vol.38, No.1, pp. 75-81

de Melo, O. N.; Fukushima, F. B.; de Matos, G. A.; Bueno, D. F.; de Oliveira, T. S. & Serakides, R. (2006). Idiopathic hypertrophic osteopathy in a cat. *J.Feline.Med.Surg.*, Vol.8, No.5, pp. 345-348

de Vries, B. B.; Pfundt, R.; Leisink, M.; Koolen, D. A.; Vissers, L. E.; Janssen, I. M.; Reijmersdal, S.; Nillesen, W. M.; Huys, E. H.; Leeuw, N.; Smeets, D.; Sistermans, E. A.; Feuth,T.; van Ravenswaaij-Arts, C. M.; van Kessel,A. G.; Schoenmakers,E. F.; Brunner, H. G. & Veltman, J. A. (2005). Diagnostic genome profiling in mental retardation. *Am.J.Hum.Genet.*, Vol.77, No.4, pp. 606-616

Deng, F. Y.; Zhao, L. J.; Pei, Y. F.; Sha, B. Y.; Liu, X. G.; Yan, H.; Wang, L.; Yang, T. L.; Recker, R. R.; Papasian, C. J. & Deng, H. W. (2010). Genome-wide copy number variation association study suggested VPS13B gene for osteoporosis in Caucasians. *Osteoporosis International*, Vol.21, No.4, pp. 579-587, ISSN/ISBN 0937-941X

Ducy, P.; Zhang, R.; Geoffroy, V.; Ridall, A. L. & Karsenty, G. (1997). Osf2/Cbfa1: A transcriptional activator of osteoblast differentiation. *Cell*, Vol.89, No.5, pp. 747-754, ISSN/ISBN 0092-8674

Feuk, L.; Carson, A. R. & Scherer, S. W. (2006). Structural variation in the human genome. *Nat.Rev.Genet.*, Vol.7, No.2, pp. 85-97

Freeman, J. L.; Perry, G. H.; Feuk, L.; Redon, R.; McCarroll, S. A.; Altshuler, D. M.; Aburatani, H.; Jones, K. W.; Tyler-Smith, C.; Hurles, M. E.; Carter, N. P.; Scherer, S. W. & Lee, C. (2006). Copy number variation: new insights in genome diversity. *Genome Res.*, Vol.16, No.8, pp. 949-961

Fuchs, S.; Hermanns, M. I. & Kirkpatrick, C. J. (2006a). Retention of a differentiated endothelial phenotype by outgrowth endothelial cells isolated from human peripheral blood and expanded in long-term cultures. *Cell Tissue Res.*, Vol.326, No.1, pp. 79-92

Fuchs, S.; Motta, A.; Migliaresi, C. & Kirkpatrick, C. J. (2006b). Outgrowth endothelial cells isolated and expanded from human peripheral blood progenitor cells as a potential source of autologous cells for endothelialization of silk fibroin biomaterials. *Biomaterials*, Vol.27, No.31, pp. 5399-5408

Gao, Y.; Sun, Y.; Ren, F., & Gao,S. (2010). PLGA-PEG-PLGA hydrogel for ocular drug delivery of dexamethasone acetate. *Drug Dev.Ind.Pharm.*, Vol.36, No.10, pp. 1131-1138

Garrett, I. R.; Gutierrez, G. E.; Rossini, G.; Nyman, J.; McCluskey, B.; Flores, A. & Mundy, G. R. (2007). Locally delivered lovastatin nanoparticles enhance fracture healing in rats. *Journal of Orthopaedic Research*, Vol.25, No.10, pp. 1351-1357, ISSN/ISBN 0736-0266

Gonzalez, E.; Kulkarni, H.; Bolivar, H.; Mangano, A.; Sanchez, R.; Catano, G.; Nibbs, R. J.; Freedman, B. I.; Quinones, M. P.; Bamshad, M.J.; Murthy, K. K.; Rovin, B.H.; Bradley, W.; Clark, R.A.; Anderson, S. A.; O'connell, R. J.; Agan, B. K.; Ahuja, S. S.; Bologna, R.; Sen, L.; Dolan, M. J. & Ahuja, S. K. (2005). The influence of CCL3L1 gene-containing segmental duplications on HIV-1/AIDS susceptibility. *Science*, Vol.307, No.5714, pp. 1434-1440

Grabo, T. & Longyhore, D. (2008). Pharmacological Management, In: *Osteoporosis: Clinical guidelines for prevention, diagnosis and management*, S. Gueldner, T. Grabo, E. Newman, D. Cooper, (Eds.), 47-82, Springer Publishing Company LLC, ISBN 13: 978-0-8261-0276-8, New York, USA

Hench, L. L. (1982). Glass Surfaces - 1982. *Journal de Physique*, Vol.43, No.NC-9, pp. 625-636, ISSN/ISBN 0302-0738

Hench, L. L. (2004). Glasses to turn on genes. *Glass Science and Technology*, Vol.77, pp. 95-103, ISSN/ISBN 0946-7475

Hopper,J.L. (2000). How to determine if, and by how much, genetic variation influences osteoporosis, In: *The genetics of osteoporosis and metabolic bone disease*, Michael J.Econs, (Ed.), 29-44, Humana Press Inc., Totowa, ISBN 0-89603-702-9, New Jersey, USA

Horiuchi, N. & Maeda, T. (2006). Statins and bone metabolism. *Oral Diseases*, Vol.12, No.2, pp. 85-101, ISSN/ISBN 1354-523X

Iafrate, A. J.; Feuk, L.; Rivera, M. N.; Listewnik, M. L.; Donahoe, P. K.; Qi, Y.; Scherer, S. W. & Lee, C. (2004). Detection of large-scale variation in the human genome. *Nat.Genet.*, Vol.36, No.9, pp. 949-951

Ivanova, L.; Popov, C.; Kolev, I.; Shivachev, B.; Karadjov, J.; Tarassov, M.; Kulisch, W.; Reithmaier, J. P. & Apostolova, M. D. (2011). Nanocrystalline diamond containing hydrogels and coatings for acceleration of osteogenesis. *Diamond and Related Materials*, Vol.20, No.2, pp. 165-169, ISSN 0925-9635

Kan, P.; Lin, X. Z.; Hsieh, M. F., & Chang, K. Y. (2005). Thermogelling emulsions for vascular embolization and sustained release of drugs. *J Biomed.Mater.Res.B Appl.Biomater.*, Vol.75, No.1, pp. 185-192

Kim, Y. J.; Choi, S.; Koh, J. J.; Lee, M.; Ko, K. S., & Kim, S. W. (2001). Controlled release of insulin from injectable biodegradable triblock copolymer. *Pharm.Res.*, Vol.18, No.4, pp. 548-550

Koch, H.; Kulisch, W.; Popov, C.; Merz, R.; Merz, B. & Reithmaier, J. P. (2011). Plasma amination of ultrananocrystalline diamond/amorphous carbon composite films for the attachment of biomolecules. *Diamond and Related Materials*, Vol.20, No.2, pp. 254-258, ISSN/ISBN 09259635

Kulisch, W. & Popov, C. (2006). On the growth mechanisms of nanocrystalline diamond films. *Physica Status Solidi (A) Applications and Materials*, Vol.203, pp.203-219

Kulisch, W.; Popov, C.; Bliznakov, S.; Ceccone, G.; Gilliland, D.; Sirghi, L. & Rossi, F. (2007). Surface and bioproperties of nanocrystalline diamond/amorphous carbon nanocomposite films. *Thin Solid Films*, Vol.515, No.23, pp. 8407-8411, ISSN/ISBN 00406090

Kulisch, W.; Popov, C.; Gilliland, D.; Ceccone, G.; Rossi, F. & Reithmaier, J. P. (2010). Investigation of the UV/O3 treatment of ultrananocrystalline diamond films. *Surface and Interface Analysis*, Vol.42, No.6-7, pp. 1152-1155, ISSN 01422421

Kulisch, W.; Popov, C.; Sasaki, T.; Sirghi, L.; Rauscher, H.; Rossi, F. & Reithmaier, J. P. (2011). On the development of the morphology of ultrananocrystalline diamond films. *Physica Status Solidi (A) Applications and Materials*, Vol.208, No.1, pp. 70-80, ISSN 18626300

Kulisch, W.; Sasaki, T.; Rossi, F.; Popov, C.; Sippel, C. & Grambole, D. (2008). Hydrogen incorporation in ultrananocrystalline diamond/amorphous carbon films. *Physica Status Solidi - Rapid Research Letters*, Vol.2, No.2, pp. 77-79, ISSN 18626254

Lee, D. S.; Shim, M. S.; Kim, S. W.; Lee, H.; Park, I. & Chang,T.Y. (2001). Novel thermoreversible gelation of biodegradable PLGA-block-PEO-block-PLGA triblock copolymers in aqueous solution. *Macromolecular Rapid Communications*, Vol.22, No.8, pp. 587-592, ISSN 1022-1336

Lee, S. U. J.; Han, B. O. R.; Park, S. Y.; Han, D. K. & Kim, S. C. (2006). Sol-gel transition behavior of biodegradable three-arm and four-arm star-shaped PLGA-PEG block copolymer aqueous solution. *Journal of Polymer Science, Part A: Polymer Chemistry*, Vol.44, No.2, pp. 888-899, ISSN 0887624X

Marini, F. & Brandi, M. L. (2010). Genetic determinants of osteoporosis: common bases to cardiovascular diseases? *International Journal of Hypertension*, Vol.2010, 16 pages-doi:10.4061/2010/394579, ISSN/ISBN 2090-0392

Moroni, A.; Faldini, C.; Marchetti, S.; Manca, M.; Consoli, V. & Giannini, S. (2001). Improvement of the bone-pin interface strength in osteoporotic bone with use of hydroxyapatite-coated tapered external-fixation pins. A prospective, randomized clinical study of wrist fractures. *J.Bone Joint Surg.Am.*, Vol.83-A, No.5, pp. 717-721

Moroni, A.; Faldini, C.; Pegreffi, F.; Hoang-Kim, A. & Giannini, S. (2005a). Osteoporotic pertrochanteric fractures can be successfully treated with external fixation. *J.Bone Joint Surg.Am.*, Vol.87 Suppl 2, pp. 42-51

Moroni, A.; Faldini, C.; Pegreffi, F.; Hoang-Kim, A.; Vannini, F. & Giannini, S. (2005b). Dynamic hip screw compared with external fixation for treatment of osteoporotic pertrochanteric fractures. A prospective, randomized study. *J.Bone Joint Surg.Am.*, Vol.87, No.4, pp. 753-759

Nguyen, M. K. & Lee, D. S. (2010). Injectable biodegradable hydrogels. *Macromol. Biosci.*, Vol.10, No.6, pp. 563-579

Niemeyer, P.; Schonberger, T. S.; Hahn, J.; Kasten, P.; Fellenberg, J.; Suedkamp, N.; Mehlhorn, A. T.; Milz, S. & Pearce, S. (2010). Xenogenic transplantation of human

mesenchymal stem cells in a critical size defect of the sheep tibia for bone regeneration. *Tissue Eng Part A*, Vol.16, No.1, pp. 33-43

Nikolovski, J. & Mooney, D. J. (2000). Smooth muscle cell adhesion to tissue engineering scaffolds. *Biomaterials*, Vol.21, No.20, pp. 2025-2032

Nordahl, J.; Mengarelliwidholm, S.; Hultenby, K. & Reinholt, F. P. (1995). Ultrastructural Immunolocalization of Fibronectin in Epiphyseal and Metaphyseal Bone of Young-Rats. *Calcified Tissue International*, Vol.57, No.6, pp. 442-449, ISSN/ISBN 0171-967X

Penrod J.; Smith A., Terwilliger S., & Gueldner S. (2008). Demographic perspective: The magnitude of concern, In: *Osteoporosis: Clinical guidelines for prevention, diagnosis and management*, S. Gueldner, T. Grabo, E. Newman, D. Cooper, (Eds.), 9-18, Springer Publishing Company LLC, ISBN 13: 978-0-8261-0276-8, New York, USA

Popov C. & Kulisch W. (2003). Investigation of nanocrystalline diamond films prepared by microwave plasma chemical vapor deposition, *Proceedings of the CVD XVI and EUROCVD-14 Conference*, pp. 1079-1085, ISBN 978-1-56677-378-2, Paris, France, October, 2003

Popov, C.; Bliznakov, S.; Boycheva, S.; Milinovik, N.; Apostolova, M. D.; Anspach, N.; Hammann, C.; Nellen, W.; Reithmaier, J. P. & Kulisch, W. (2008a). Nanocrystalline diamond/amorphous carbon composite coatings for biomedical applications. *Diamond and Related Materials*, Vol.17, No.4-5, pp. 882-887, ISSN/ISBN 09259635

Popov, C.; Kulisch, W.; Bliznakov, S.; Ceccone, G.; Gilliland, D.; Sirghi, L. & Rossi, F. (2008b). Surface modification of nanocrystalline diamond/amorphous carbon composite films. *Diamond and Related Materials*, Vol.17, No.7-10, pp. 1229-1234, ISSN/ISBN 09259635

Popov, C., Kulisch, W., Boycheva, S. & Jelinek, M. (2003). Nanocrystalline diamond/ amorphous carbon composite films prepared by MWCVD, *Proceedings of the International Conference on Nanosciences, Nanotechnologies and Nanomaterials NANO '03*, pp. 148-153, ISBN 80-214-2525-X, Brno, Czech Republic, October, 2003

Popov, C.; Kulisch, W.; Gibson, P. N.; Ceccone, G. & Jelinek, M. (2004). Growth and characterization of nanocrystalline diamond/amorphous carbon composite films prepared by MWCVD. *Diamond and Related Materials*, Vol.13, No.4-8, pp. 1371-1376, ISSN/ISBN 09259635

Popov, C.; Kulisch, W.; Jelinek, M.; Bock, A. & Strnad, J. (2006a). Nanocrystalline diamond/amorphous carbon composite films for applications in tribology, optics and biomedicine. *Thin Solid Films*, Vol.494, No.1-2, pp. 92-97, ISSN/ISBN 00406090

Popov, C.; Kulisch, W.; Reithmaier, J. P.; Dostalova, T.; Jelinek, M.; Anspach, N. & Hammann, C. (2007). Bioproperties of nanocrystalline diamond/amorphous carbon composite films. *Diamond and Related Materials*, Vol.16, No.4-7 SPEC. ISS., pp. 735-739, ISSN/ISBN 09259635

Popov, C.; Novotny, M.; Jelinek, M.; Boycheva, S.; Vorlicek, V.; Trchova, M. & Kulisch, W. (2006b). Chemical bonding study of nanocrystalline diamond films prepared by plasma techniques. *Thin Solid Films*, Vol.506-507, pp. 297-302, ISSN 00406090

Popov, C.; Vasilchina, H.; Kulisch, W.; Danneil, F.; Stüber, M.; Ulrich, S.; Welle, A. & Reithmaier, J. P. (2009). Wettability and protein adsorption on ultrananocrystalline diamond/amorphous carbon composite films. *Diamond and Related Materials*, Vol.18, No.5-8, pp. 895-898, ISSN 09259635

Popov, C.; Kulisch, W.; Boycheva, S.; Yamamoto, K.; Ceccone, G. & Koga, Y. (2004). Structural investigation of nanocrystalline diamond/amorphous carbon composite films. *Diamond and Related Materials*, Vol.13, No.11-12, pp. 2071-2075, ISSN 09259635

Popov C. & Kulisch W. (2011). Nanocrystalline diamond films for biosensor applications, In: *Nanotechnological basis for advanced sensors*, J.P. Reithmaier, P. Paunovic, W. Kulisch, C. Popov, P. Petkov (Eds.), 447-469, Springer, ISBN 978-94-007-0905-8, Dordrecht, Netherlands

Pramatarova, L.; Pecheva, E.; Stavrev, S.; Spasov, T.; Montgomery, P.; Toth, A.; Dimitrova, M., & Apostolova, M. (2007). Artificial bones through nanodiamonds. *Journal of Optoelectronics and Advanced Materials*, Vol.9, No.1, pp. 236-239, ISSN 1454-4164

Qiao, M.; Chen, D.; Ma, X., & Hu, H. (2006). Sustained release of bee venom peptide from biodegradable thermosensitive PLGA-PEG-PLGA triblock copolymer-based hydrogels in vitro. *Pharmazie*, Vol.61, No.3, pp. 199-202

Ralston, S. H. & de Crombrugghe B. (2006). Genetic regulation of bone mass and susceptibility to osteoporosis. *Genes Dev.*, Vol.20, No.18, pp. 2492-2506

Redon, R.; Ishikawa, S.; Fitch, K. R.; Feuk, L.; Perry, G. H.; Andrews, T. D.; Fiegler, H.; Shapero, M. H.; Carson, A. R.; Chen, W.; Cho, E. K.; Dallaire, S.; Freeman, J. L.; Gonzalez, J. R.; Gratacos, M.; Huang, J.; Kalaitzopoulos, D.;Komura,D.; MacDonald, J. R.; Marshall, C. R.; Mei, R.; Montgomery, L.; Nishimura, K.; Okamura, K.; Shen, F.; Somerville, M. J.; Tchinda, J.; Valsesia, A.; Woodwark, C.; Yang, F.; Zhang, J.; Zerjal, T.; Zhang, J.; Armengol, L.; Conrad, D. F.; Estivill, X.; Tyler-Smith, C.; Carter, N. P.; Aburatani, H.; Lee, C.; Jones, K. W.; Scherer, S. W. & Hurles, M. E. (2006). Global variation in copy number in the human genome. *Nature*, Vol.444, No.7118, pp. 444-454

Repping, S.; van Daalen, S. K.; Brown, L. G.; Korver, C. M.; Lange, J.; Marszalek, J. D.; Pyntikova, T.; van, der, V; Skaletsky, H.; Page, D. C. & Rozen, S. (2006). High mutation rates have driven extensive structural polymorphism among human Y chromosomes. *Nat.Genet.*, Vol.38, No.4, pp. 463-467

Richards, J. B.; Kavvoura, F. K.; Rivadeneira, F.; Styrkarsdottir, U.; Estrada, K.; Halldorsson, B.V.; Hsu, Y. H.; Zillikens, M. C.; Wilson, S. G.; Mullin, B. H.; Amin, N.; Aulchenko, Y. S.; Cupples, L.A.; Deloukas, P.; Demissie, S.; Hofman, A.; Kong, A.; Karasik, D.; van Meurs, J. B.; Oostra, B. A.; Pols, H. A.; Sigurdsson, G.; Thorsteinsdottir, U.; Soranzo, N.; Williams, F. M.; Zhou, Y.; Ralston, S. H.; Thorleifsson, G.; van Duijn, C. M.; Kiel, D. P.; Stefansson, K.; Uitterlinden, A. G.; Ioannidis, J. P. & Spector, T. D. (2009). Collaborative meta-analysis: associations of 150 candidate genes with osteoporosis and osteoporotic fracture. *Ann.Intern.Med.*, Vol.151, No.8, pp. 528-537

Robey P. (1996). Bone matrix proteoglycans and glycoproteins, In: *Principles of Bone Biology*, J. Bilezidian, L. Raisz, G. Rodan, (Eds.), 155-166, Academic Press, ISBN 0-12-098650-7, San Diego, USA

Rozen, N.; Bick, T.; Bajayo, A.; Shamian, B.; Schrift-Tzadok, M.;Gabet,Y.; Yayon, A.; Bab, I.; Soudry, M. & Lewinson, D. (2009). Transplanted blood-derived endothelial progenitor cells (EPC) enhance bridging of sheep tibia critical size defects. *Bone*, Vol.45, No.5, pp. 918-924

Schoumans, J.; Ruivenkamp, C.; Holmberg, E.; Kyllerman, M.; Anderlid, B. M. & Nordenskjold, M. (2005). Detection of chromosomal imbalances in children with idiopathic mental retardation by array based comparative genomic hybridisation (array-CGH). *J.Med.Genet.*, Vol.42, No.9, pp. 699-705

Sebat, J.; Lakshmi, B.; Malhotra, D.; Troge, J.; Lese-Martin, C.; Walsh, T.; Yamrom, B.; Yoon, S.; Krasnitz, A.; Kendall, J.; Leotta, A.; Pai, D.; Zhang, R.; Lee, Y. H.; Hicks, J.; Spence, S. J.; Lee, A. T.; Puura, K.; Lehtimaki, T.; Ledbetter, D.; Gregersen, P. K.; Bregman, J.; Sutcliffe, J. S.; Jobanputra, V.; Chung, W.; Warburton, D.; King, M. C.; Skuse, D.;

Geschwind, D. H.; Gilliam, T. C.; Ye, K. & Wigler, M. (2007). Strong association of de novo copy number mutations with autism. *Science*, Vol.316, No.5823, pp. 445-449

Sebat, J.; Lakshmi, B.; Troge, J.; Alexander, J.; Young, J.; Lundin, P.; Maner, S.; Massa, H.; Walker, M.; Chi, M.; Navin, N.; Lucito, R.; Healy, J.; Hicks, J.; Ye, K.; Reiner, A.; Gilliam, T. C.; Trask, B.; Patterson, N.; Zetterberg, A. & Wigler,M. (2004). Large-scale copy number polymorphism in the human genome. *Science*, Vol.305, No.5683, pp. 525-528

Sharp, A. J.; Locke, D. P.; McGrath, S. D.; Cheng, Z.; Bailey, J. A.; Vallente, R. U.; Pertz, L. M.; Clark, R. A.; Schwartz, S.; Segraves, R.; Oseroff, V. V.; Albertson, D. G.; Pinkel,D. & Eichler, E. E. (2005). Segmental duplications and copy-number variation in the human genome. *Am.J.Hum.Genet.*, Vol.77, No.1, pp. 78-88

Shih, C.; Waldron, N. & Zentner, G. M. (1996). Quantitative analysis of ester linkages in poly(DL-lactide) and poly(DL-lactide-co-glycolide). *Journal of Controlled Release*, Vol.38, No.1, pp. 69-73, ISSN 0168-3659

Trajkovski, B.; Karadjov, J., Shivachev, B., Dimitrova, A., Stavrev, S. & Apostolova, M. D. (2009). Novel nanostructured materials accelerating osteogenesis, In: *Nanostructured Materials for Advanced Technological Applications,* J. P. Reithmaier, P. Petkov, W. Kulisch, C. Popov, (Eds.), 525-532, Springer, ISBN 978-1-4020-9915-1, Dordrecht, Netherlands

Tsoncheva, T.; Ivanova, L.; Paneva, D.; Dimitrov, M.; Mitov, I.; Stavrev, S. & Minchev, C. (2006). Iron-oxide-modified nanosized diamond: preparation, characterization, and catalytic properties in methanol decomposition. *J.Colloid Interface Sci.*, Vol.302, No.2, pp. 492-500

Tuzun, E.; Sharp, A. J.; Bailey, J. A.; Kaul, R.; Morrison, V. A.; Pertz, L. M.; Haugen, E.; Hayden, H.; Albertson, D.; Pinkel, D.; Olson, M. V. & Eichler, E. E. (2005). Fine-scale structural variation of the human genome. *Nat.Genet.*, Vol.37, No.7, pp. 727-732

Wei, G. & Ma, P. X. (2007). Polymeric biomaterials, In: *Tissue engineering using ceramics and polymers*, A. Boccaccini, J. Gough (Eds.), 32-50, Woodhead Publishing Limited, ISBN 978-1-84569-176-9, England, Cambridge

Woll, N. L. & Bronson, S. K. (2006). Analysis of embryonic stem cell-derived osteogenic cultures. *Methods Mol.Biol.*, Vol.330, pp. 149-159

Woll, N. L.; Heaney, J. D. & Bronson, S. K. (2006). Osteogenic nodule formation from single embryonic stem cell-derived progenitors. *Stem Cells Dev.*, Vol.15, No.6, pp. 865-879

Youxin, L.; Volland, C. & Kissel, T. (1994). In-vitro degradation and bovine serum albumin release of the ABA triblock copolymers consisting of poly(L(+)lactic acid), or poly(L(+)lactic acid-co-glycolic acid) A-blocks attached to central polyoxyethylene B-blocks. *Journal of Controlled Release*, Vol.32, No.2, pp. 121-128, ISSN/ISBN 01683659

Yu, L.; Zhang, Z.; Zhang, H. & Ding, J. (2010). Biodegradability and biocompatibility of thermoreversible hydrogels formed from mixing a sol and a precipitate of block copolymers in water. *Biomacromolecules.*, Vol.11, No.8, pp. 2169-2178

Zentner, G. M.; Rathi, R.; Shih, C.; McRea, J. C.; Seo, M. H.; Oh, H.; Rhee, B. G.; Mestecky, J.; Moldoveanu, Z.; Morgan, M., & Weitman,S. (2001). Biodegradable block copolymers for delivery of proteins and water-insoluble drugs. *J Control Release*, Vol.72, No.1-3, pp. 203-215

Zhang, Y. P.; Deng, F. Y.; Chen, Y.; Pei, Y. F.; Fang, Y.; Guo Y. F.; Guo X.; Liu X. G.; Zhou, Q.; Liu Y. J. & Deng, H. W. (2010). Replication study of candidate genes/loci associated with osteoporosis based on genome-wide screening. *Osteoporos.Int.,* Vol.21, pp.785-795

Zweers, M. L.; Engbers, G. H.; Grijpma, D. W. & Feijen, J. (2004). In vitro degradation of nanoparticles prepared from polymers based on DL-lactide, glycolide and poly(ethylene oxide). *J Control Release*, Vol.100, No.3, pp. 347-356

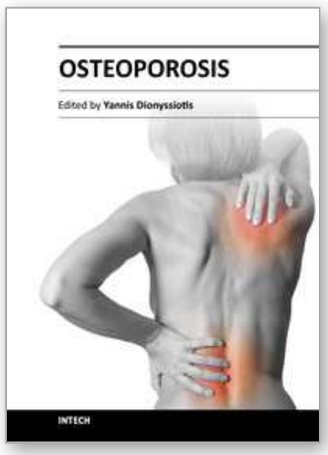

Osteoporosis

Edited by PhD. Yannis Dionyssiotis

ISBN 978-953-51-0026-3
Hard cover, 864 pages
Publisher InTech
Published online 24, February, 2012
Published in print edition February, 2012

Osteoporosis is a public health issue worldwide. During the last few years, progress has been made concerning the knowledge of the pathophysiological mechanism of the disease. Sophisticated technologies have added important information in bone mineral density measurements and, additionally, geometrical and mechanical properties of bone. New bone indices have been developed from biochemical and hormonal measurements in order to investigate bone metabolism. Although it is clear that drugs are an essential element of the therapy, beyond medication there are other interventions in the management of the disease. Prevention of osteoporosis starts in young ages and continues during aging in order to prevent fractures associated with impaired quality of life, physical decline, mortality, and high cost for the health system. A number of different specialties are holding the scientific knowledge in osteoporosis. For this reason, we have collected papers from scientific departments all over the world for this book. The book includes up-to-date information about basics of bones, epidemiological data, diagnosis and assessment of osteoporosis, secondary osteoporosis, pediatric issues, prevention and treatment strategies, and research papers from osteoporotic fields.

How to reference

In order to correctly reference this scholarly work, feel free to copy and paste the following:

Iliyan Kolev, Lyudmila Ivanova, Leni Markova, Anelia Dimitrova, Cyril Popov and Margarita D. Apostolova (2012). Osteoporosis: A Look at the Future, Osteoporosis, PhD. Yannis Dionyssiotis (Ed.), ISBN: 978-953-51-0026-3, InTech, Available from: http://www.intechopen.com/books/osteoporosis/osteoporosis-a-look-at-the-future

INTECH
open science | open minds

InTech Europe
University Campus STeP Ri
Slavka Krautzeka 83/A
51000 Rijeka, Croatia
Phone: +385 (51) 770 447
Fax: +385 (51) 686 166
www.intechopen.com

InTech China
Unit 405, Office Block, Hotel Equatorial Shanghai
No.65, Yan An Road (West), Shanghai, 200040, China
中国上海市延安西路65号上海国际贵都大饭店办公楼405单元
Phone: +86-21-62489820
Fax: +86-21-62489821

IntechOpen